A Lagrangian Analysis of the Atmospheric Branch of the Global Water Cycle. Part I: Method Description, Validation, and Demonstration for the August 2002 Flooding in Central Europe

ANDREAS STOHL

Cooperative Institute for Research in Environmental Sciences, NOAA/Aeronomy Laboratory, University of Colorado, Boulder, Colorado

PAUL JAMES

Department of Bioclimatology, Technical University of Munich, Munich, Germany

(Manuscript received 2 November 2003, in final form 28 February 2004)

ABSTRACT

Understanding and quantifying the relationships between evaporation of water in one region, precipitation in another, and the transport processes connecting them, is one of the key problems in hydrometeorology. However, to date few methods exist that are suitable for establishing these relationships. In this paper, a new Lagrangian technique is described that builds on methods that have been developed for investigating source–receptor relationships for air pollutants. It is based on meteorological analysis data and a particle dispersion model and uses a Lagrangian analog to the Eulerian budget method to diagnose the surface moisture flux. Because of its Lagrangian nature, regions of net evaporation are connected by trajectories with regions of net precipitation, and these trajectories can be used to examine how the two are related. The method is shown to yield estimates for the global distribution of the annual mean surface freshwater flux that are equally accurate as those obtained with the Eulerian budget method. It is then applied in a case study of an extreme precipitation event that occurred in central Europe in August 2002 and led to floodings with return periods of 100 to 300 yr in some river catchments. Again it is shown that the moisture fluxes obtained with the Lagrangian and Eulerian method, respectively, agree well with each other, and both agree well with observed precipitation patterns and short-range precipitation forecasts. Then the new method is used to determine where the water that became precipitation during the flooding event has evaporated. It is found that in addition to a strong Mediterranean source, much of the water evaporated from land. The strong extra evaporation over land was likely due to a wet spell the weeks before that left soils saturated with water in large parts of Europe and flooded in some smaller regions. It appears that precipitation forecasts suffered from predicting too little evaporation in these regions.

1. Introduction

Water is essential for life on earth and is a key factor in the climate system. Phase transitions, which couple the earth's atmosphere, hydrosphere, biosphere, and cryosphere, are critical for stabilizing the earth's climate at temperatures near water's triple point (Webster 1994). Water vapor is the most important greenhouse gas in the atmosphere (e.g., Houghton et al. 2001), and it also influences the climate system's sensitivity to changes in other greenhouse gases (Schneider et al. 1999). Water furthermore modifies the earth's radiation budget through cloud formation. Redistribution of latent heat by water vapor transport is an important factor for the global atmospheric energy balance (Peixoto and Oort 1992). Water also influences the biogeochemical cycles of many elements, for instance, of carbon via a strong coupling between transpiration and CO_2 uptake during photosynthesis (Lee and Veizer 2003).

Yet, even such important components of the hydrologic cycle as the spatiotemporal distribution of evapotranspiration (E) and precipitation (P), are not known with satisfactory accuracy. Reasons for this are the lack of observations particularly over the oceans, the high variability of these parameters, leading to poor representativity of point measurements, and measurement difficulties. The Global Precipitation Climatology Project (GPCP) (Huffman et al. 1997) has combined a number of different types of products, both from rain gauge and satellite data, to monthly (Huffman et al. 1997) and daily (Huffman et al. 2001) global fields of P. The GPCP data contain relatively large uncertainties, particularly on a daily basis. A correlation with Pacific atoll gauge measurements shows considerable scatter and suggests that the GPCP data may be biased low by 16% in this

Corresponding author address: Dr. Andreas Stohl, Cooperative Institute for Research in Environmental Sciences, University of Colorado, NOAA/Aeronomy Laboratory, R/AL4, Room 2A101, 325 Broadway, Boulder, CO 80305.
E-mail: Andreas.Stohl@noaa.gov

region (Adler et al. 2003). However, for E the situation is even worse, because no global observations exist at all.

Predictions by weather forecast models can substitute measurements of E and P. However, the quality of predicted E and P depends critically on the forecast model's physical realism and the validity of its parameterizations. In fact, serious problems exist with forecast moisture fluxes (e.g., Trenberth and Guillemot 1998) and, because of model spinup, they systematically depend on the forecast time.

An alternative to both forecasts and direct observations of E and P is to derive net ($E - P$) surface moisture fluxes indirectly as a residual from the budget of water vapor in an atmospheric column, using the principle of mass conservation (Trenberth 1997). This method has the advantage that all variables needed to solve the budget equation for $E - P$ are observeable with relatively good accuracy and are available from meteorological analyses. Its reliability depends on the accuracy of the assimilated water vapor, wind, and pressure data that enter the budget equation (Trenberth and Guillemot 1998).

In this paper we present a Lagrangian analog to the Eulerian budget method, using a particle dispersion model. The major advantage of the Lagrangian approach is not an improved accuracy compared to its Eulerian equivalent. In fact, we show that the two methods yield practically identical results. But the Lagrangian method has the advantage that these budgets can be traced along suitably defined trajectory ensembles, thereby facilitating the determination of source–receptor relationships of water.

Where did all the water come from? This is perhaps the most puzzling question to be posed for precipitation generally, and for extreme rain events in particular. Trenberth et al. (2003) discussed the fact that only a minor fraction of the water converted into precipitation in a storm system originates locally, that is, evaporates into the storm itself, whereas most of it is supplied by outside sources and is transported into the storm. Newell et al. (1992) identified atmospheric bands with especially large horizontal water vapor fluxes, which they termed ''tropospheric rivers'' because both their length scale and amount of water transported are as large as those of the Amazon River. These rivers supply the moisture for warm conveyor belts, the major precipitating cloud systems of extratropical cyclones (Eckhardt et al. 2004). Despite the recognition of the importance of water vapor transport, surprisingly few studies have been conducted to answer the question stated at the beginning of this paragraph, neither on a case study basis, nor climatologically. We perhaps know more about the transport of some minor trace gases (e.g., Stohl et al. 2003) than we know about water vapor transport, mainly because few methods can reliably account for precipitation and evaporation occurring en route.

Global maps of the divergent part of the water vapor flux give an idea about the flow of moisture from the major subtropical centers of strong evaporation to the tropical and midlatitude centers of precipitation (Chen and Pfaendtner 1993), but they cannot identify the actual pathways of the water vapor. Water vapor evaporating from different source regions differs in its isotopic composition, which therefore can give information on where rainwater has originated (e.g., Yamanaka et al. 2002). Unfortunately, isotope data are not normally available. Some theoretical studies considered only the local recycling of precipitation (Eltahir and Bras 1996) but did not locate the moisture sources outside the region considered. Regional water vapor tracers have been used in general circulation models to explore where the water fallen as precipitation in a target area has evaporated (Koster et al. 1986; Bosilovich and Schubert 2002; Bosilovich et al. 2003). However, this approach is sensitive to errors in the simulation of the hydrologic cycle. Furthermore, the regions where water vapor tracers are sourced must be prespecified, requiring a priori information on the distribution of sources relevant for the study area. In other studies, trajectories have been used to examine the pathways of the air masses that produced the precipitation (e.g., D'Abreton and Tyson 1996; Crimp and Mason 1999). But while trajectories may help identifying where an air mass did come from, they per se fail to diagnose evaporation and, thus, remain qualitative. In a case study, however, Wernli (1997) used the decrease of specific humidity along a trajectory to estimate precipitation rates. Recently, Dirmeyer and Brubaker (1999) and Brubaker et al. (2001) developed an interesting trajectory approach to identify moisture source regions. But their approach also has a number of weaknesses, like the use of not fully consistent data (observed precipitation, simulated evapotranspiration), and it cannot identify those air parcels in a vertical column actually producing the precipitation. It also does not account for the fact that an air parcel may eventually undergo a series of evaporation and precipitation cycles before arriving in the target region. Nevertheless, this is an innovative method for identifying water vapor source regions (e.g., Reale et al. 2001).

In this paper we present a Lagrangian analog of the Eulerian budget method (Trenberth 1997). It is quantitative, builds only on analyzed meteorological data (instead of GCM simulations), and allows for the tracking of moisture. The paper is organized in the following way: In the next section, we explain the method and present the data and model used. In section 3 we compare the surface moisture fluxes obtained with the new method with other data, both globally and in a regional case study. In section 4 we demonstrate our method of tracking moisture from evaporation to precipitation at the example of a flooding event over Europe, and in section 5 we draw conclusions. A companion paper (A. Stohl et al. 2004, unpublished manuscript) will explore global relationships between evaporation and precipitation.

2. Methods

a. E, P, and E − P diagnostics

If we ignore the presence of liquid water and ice in the atmosphere, the water budget in an atmospheric column can be written as

$$E - P = \frac{\partial w}{\partial t} + \nabla \cdot \frac{1}{g} \int_0^{p_s} q\mathbf{v}\, dp, \tag{1}$$

where $E - P$ is the surface freshwater flux, $w = 1/g \int_0^{p_s} q\, dp$ is the precipitable water, t is time, g is the gravitational acceleration, q is the specific humidity, $\mathbf{v}$ is the wind, and E is the evaporation and P the precipitation rate per unit area (Trenberth and Guillemot 1998). All of the terms on the right-hand side of (1) can be evaluated from global analyses. See Trenberth (1997) for a discussion of the uncertainties of (1). Hereinafter we refer to (1) as the Eulerian method, which we use as a standard against which $E - P$ estimates from our new method are compared.

For implementing a Lagrangian analog to (1) we start by dividing the atmosphere into a large number N of so-called particles, which are homogeneously distributed such that their number density is proportional to the air density. Given a total atmospheric mass m_a, each particle therefore represents a mass $m = m_a/N$. A particle is then advected using the trajectory equation

$$\frac{d\mathbf{x}}{dt} = \mathbf{v}[\mathbf{x}(t)], \tag{2}$$

where $\mathbf{x}$ is the particle's position, and $\mathbf{v}[\mathbf{x}(t)]$ is the wind velocity interpolated in space and time from the analysis grid to $\mathbf{x}(t)$.

By interpolating q to $\mathbf{x}(t)$, the net rate of change of the water vapor content of a particle becomes

$$e - p = m\frac{dq}{dt}, \tag{3}$$

where e and p are the rates of moisture increases and decreases along the trajectory, respectively. Figure 1 shows a sketch of the trajectory of a particle undergoing an evaporation–precipitation cycle, and the associated diagnostics. In analogy to the widely used form of (1), e and p are kept as separate terms in (3), although—like (1)—it can be used only to diagnose their net effect. A small error is introduced here because the mass of a particle (and, thus, also the mass of the whole atmosphere) is assumed to be constant. In reality, however, the atmosphere's mass changes slightly through the addition and removal of water.

To diagnose the surface freshwater flux in an area A, the moisture changes of all particles in the atmospheric column over A are amassed, giving

$$E - P \approx \frac{\sum_{k=1}^{K} (e - p)}{A}, \tag{4}$$

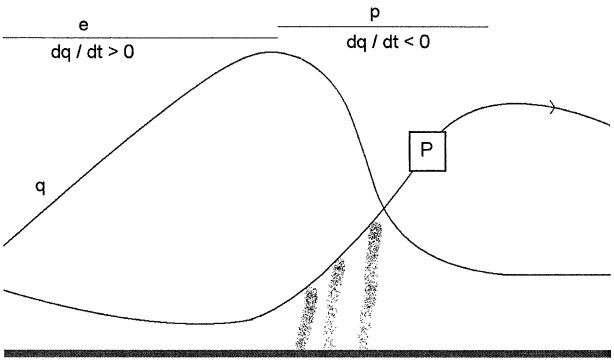

FIG. 1. Sketch of a particle undergoing an evaporation–precipitation cycle. The particle is marked with a boxed "P," and its trajectory, marked with an arrow, is assumed to first slightly descend close to the surface and then strongly ascend. The line marked with "q" is the assumed variation of q in the particle. It first increases and then, during the particle's steep ascent, decreases. Given this variation of q, $dq/dt > 0$ during the first half of the trajectory, leading to the diagnosis of net evaporation $e - p > 0$ ($e > 0$ and $p = 0$). During the trajectory's ascent, $dq/dt < 0$, leading to the diagnosis of net precipitation $e - p < 0$ ($p > 0$ and $e = 0$). Tilting shafts indicate precipitation.

where K is the number of particles residing over A. Equation (4) is a statistical relationship and is accurate only for large K, which means that either N (because K scales with N), or A, or both, must be large. Equation (4) approaches (1) when the number of particles per grid column of the analysis data exceeds the number of model layers.

Equations (1) and (4) can diagnose $E - P$, but not E or P individually. At any given time, however, precipitation occurs only on about 6% of the globe (Trenberth et al. 2003), whereas evapotranspiration is potentially active everywhere and always. On the other hand, when rain falls, it normally clearly exceeds evaporation. Therefore, by assuming that E and P cannot coexist in the same location at the same time, instantaneous rates of evaporation $E_i = E - P$ when $E - P > 0$, or precipitation $P_i = P - E$ when $E - P < 0$, can be diagnosed. Summing E_i and P_i, diagnosed for individual time steps, over a longer time period, say, a year, leads to estimates for $\overline{E}$ and $\overline{P}$, where the overbar indicates a time average.

Intuitively it may be expected that separation of E and P leads to underestimates for both quantities. However, a potentially serious problem is that liquid water and ice are neglected in (3). Phase changes in clouds are, therefore, also included in $e - p$ estimates. Taking the case shown in Fig. 1, if cloud water that formed during ascent would remain in the atmosphere and reevaporate during descent, negative $e - p$ values were enhanced upon ascent, and $e - p$ values were positive rather than zero upon descent (the last trajectory segment in Fig. 1), compared to the case where all condensed water precipitates out immediately. Values of $\overline{E - P}$, summed over the period where clouds form and evaporate, are not affected, but separating $\overline{E}$ and $\overline{P}$ leads

to the diagnosis of extra precipitation upon cloud formation and surface evaporation upon evaporation of cloud droplets. Thus, both $\overline{E}$ and $\overline{P}$ would be overestimated. Note that if water is transported across grid column boundaries in liquid or solid form, $\overline{E - P}$ estimates for individual grid columns would also be affected (the same is also true for the Eulerian method), but this is a relatively minor problem.

Another problem is that q fluctuations along individual trajectories also occur for nonphysical reasons (e.g., because of q interpolation or trajectory errors) and, consequently, absolute values of $e - p$ are biased high. Partly, such noise compensates among the many particles in an atmospheric column over area A, such that the problem is less pronounced for instantaneous $E - P$ values, but as we will see, diagnosing E and P separately still leads to overestimates for both.

If diagnosis of $E - P$ were the sole purpose of our method, particles could be redistributed to a regular grid before every time step. In order to establish meaningful source–receptor relationships, however, trajectories must be continuous over the time period of interest. In order for (4) to still work in this case, the particle distribution must fulfill, at any time, the well-mixed criterion. This criterion, a consequence of the second law of thermodynamics, states that particles that are initially well mixed must remain that way (Thomson 1987). When particles accumulate in some regions of the atmosphere and leave behind voids in others, the particle's number density is not proportional anymore to the density of air and the well-mixed criterion is violated. The well-mixed criterion imposes stringent requirements on the mass balance of the wind fields, the numerical scheme, and the turbulence statistics for trajectory calculations (Lin et al. 2003). The model used for that purpose is version 5.1 of FLEXPART, which is described in the next subsection. In FLEXPART, particles retain an almost homogeneous distribution, even for decadal model integrations (James et al. 2003).

b. Description of the Lagrangian model

FLEXPART (Stohl et al. 1998; Stohl and Thomson 1999; http://www.forst.tu-muenchen.de/EXT/LST/METEO/stohl/) was originally developed to simulate the dispersion of dangerous substances from point sources (e.g., radionuclides released during an accident in a nuclear power plant). For this type of application it was validated with data from continental-scale tracer experiments, where an inert chemical substance was released from a point and its concentration after the release was measured at many surface stations (Stohl et al. 1998). FLEXPART's applications were then extended to case studies of intercontinental air pollution transport (e.g., Stohl and Trickl 1999; Stohl et al. 2003), long-range transport of pollution from forest fires (Forster et al. 2001; Spichtinger et al. 2001), and studies of global pollution transport on climatic time scales (e.g., Stohl et al. 2002; Eckhardt et al. 2003). It was also used as a forecast tool for flight planning during field missions (Forster et al. 2004). Recently, a Lagrangian study of stratosphere–troposphere exchange was completed using FLEXPART (James et al. 2003). Most of these papers also contain some validation aspects. For a description of the theory of particle models see, for instance, the monograph by Rodean (1996).

FLEXPART uses global data with $1^\circ \times 1^\circ$ resolution from the European Centre for Medium-Range Weather Forecasts (ECMWF; White 2002) on 60 model levels. There are approximately 14 model levels below 1500 m and 23 below 5000 m. We use analyses every 6 h (at 0000, 0600, 1200, and 1800 UTC), and 3-h forecasts at intermediate times (at 0300, 0900, 1500, and 2100 UTC). The 3-h forecasts are used here to supplement the analyses because the time resolution is critical for the accuracy of Lagrangian trajectories (Stohl et al. 1995). A sensitivity study using only the analyses yielded almost identical results, though, for the $E - P$ estimates. To ensure exact mass balance, vertical winds are calculated using spherical harmonics data as part of the data-retrieval procedures at ECMWF.

FLEXPART calculates particle trajectories using analyzed winds plus random motions in order to account for turbulence. In the planetary boundary layer (PBL), these random motions are calculated by solving Langevin equations for Gaussian turbulence (Stohl and Thomson 1999). These equations use the Lagrangian time scales and the standard deviations of the wind components, which are computed from ECMWF PBL parameters (Hanna 1982). The PBL height is diagnosed using a combined Richardson number and lifting parcel technique (Vogelezang and Holtslag 1996). Outside the PBL, turbulence is assumed to be very small.

Global datasets also do not resolve individual convective cells, although they reproduce the large-scale effects of convection, for example, slantwise convection in extratropical cyclones. To account for subgrid-scale convective transport, FLEXPART uses the convection scheme developed by Emanuel and Živković-Rothman (1999). It was not used here because it redistributes particles only within a single column. This conserves precipitable water and, thus, does not affect $E - P$ diagnostics. For tracking moisture, it will become important because it changes the particles' trajectories. However, further tests on its effect on the q changes along trajectories are required before it can be applied in this context.

FLEXPART has different options for how particles are generated and what they represent (air, or a certain trace gas that might be emitted during the simulation). Here, at the model's start, the atmosphere was ''filled'' homogeneously with particles, each representing a fraction of the total atmospheric mass. Particles were then allowed to move freely (forward in time, but this is arbitrary) with the winds for the duration of the simulation. In the case study of the flooding event, when we

a) E - P from ECMWF forecast

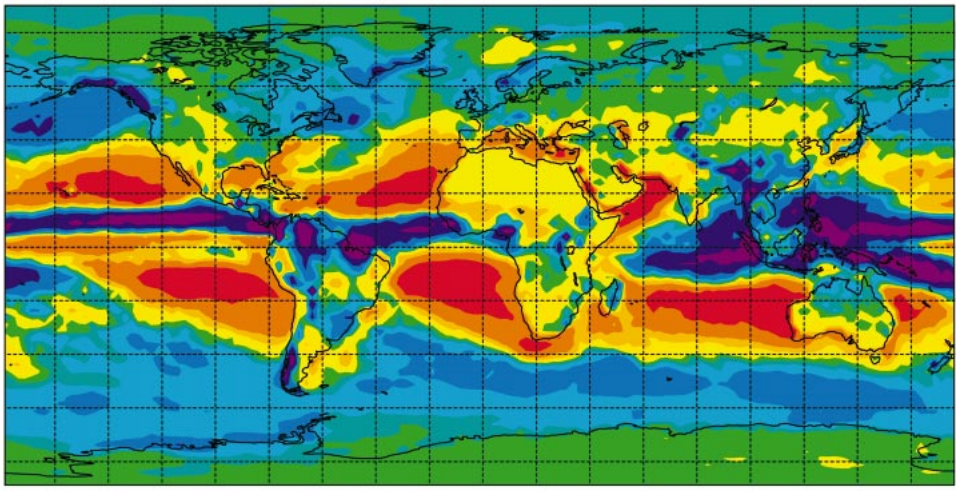

b) E - P from Eulerian diagnostic

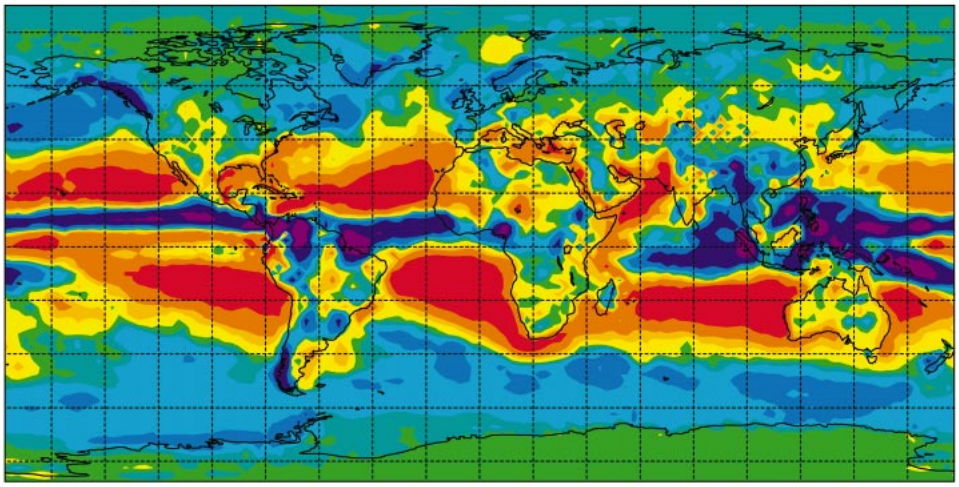

c) E - P from Lagrangian diagnostic

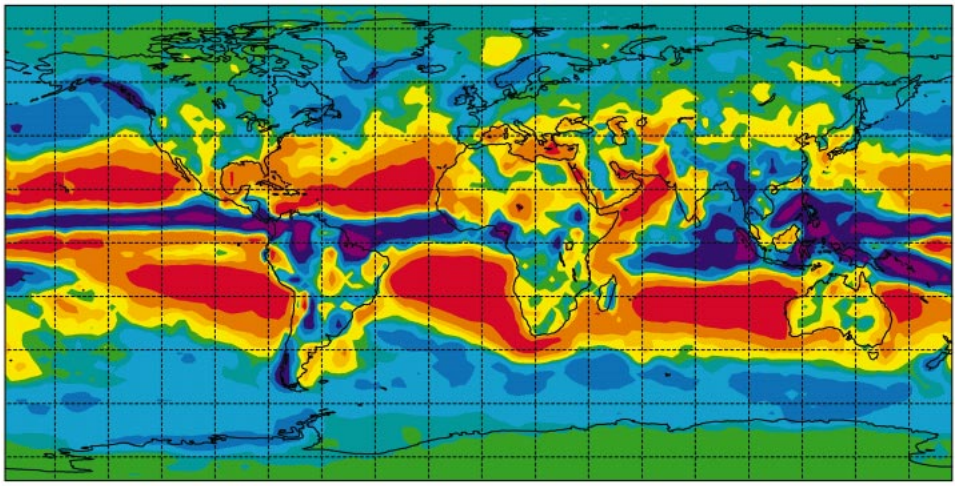

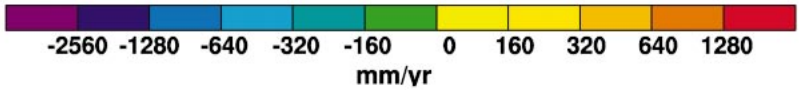

used a limited simulation domain, particles were generated continuously at the inflowing boundaries and were destroyed at the outflowing boundaries. Particle positions and interpolated q values were recorded in output files every 3 h (every hour for the case study), and $e - p$ was diagnosed from a particle's q change between two output times and was assigned to the particle's central position during the time step.

3. Results: *E*, *P*, and $E - P$ diagnostics

In this section, the Lagrangian diagnostics for E, P, and $E - P$ are validated on a global scale for the year 2000 and on a regional scale for a flooding event in 2002. They are compared with results obtained with the Eulerian method [(1)], which was implemented on the same ECMWF model-level data. Furthermore, both diagnostic methods are compared with 24-h operational ECMWF forecasts of E and P. Finally, P fields of version 2 from GPCP (Adler et al. 2003) are used as an independent source of data. The GPCP data were available on a $2.5^\circ \times 2.5^\circ$ grid and a monthly basis for the 1-yr study, and on a $1^\circ \times 1^\circ$ grid and a daily basis for the case study. For consistency, all results will be presented at 2.5° and 1° resolution for the 1-yr study and the case study, respectively. Moisture tracking will be demonstrated in section 4.

a. One-year global study

FLEXPART was started on 31 December 1999 with 800 000 particles, which were continuously advected until 1 January 2001. With 800 000 particles, on average 77 particles reside in every grid column, exceeding the number of model levels, 60. Figure 2 compares the distributions of the annual mean surface freshwater flux $E - P$ for the year 2000 obtained from 24-h forecasts, the Eulerian method [(1)], and the Lagrangian method [(4)]. All three methods reproduce the main global surface freshwater flux features known from previous studies (e.g., Trenberth 1997; Trenberth and Guillemot 1998). Precipitation surplusses are found around the mean position of the ITCZ and at high latitudes, separated by precipitation deficits mainly in the subtropics.

The correlation between the Lagrangian and the Eulerian diagnostics is excellent (Fig. 3a), with no bias and an explained variance of 94%—despite the fact that the two methods use shifted output grids. Even small-scale patterns, such as the high spatial variability between precipitation surplusses and deficits over Africa, are very similar. Small differences are found in a few regions. The Eulerian method gives a few isolated precipitation deficits over Antarctica, which do not appear in the Lagrangian results. With the relatively long time step of 3 h, the Lagrangian diagnostic fails to resolve small-scale features in high-latitude regions where grid cells are small and wind speeds are high. Over parts of Siberia the Eulerian method shows meshlike patterns with a length scale of two grid cells, which are likely artifacts resulting from an inaccurate numerical implementation of (1). Here, the Lagrangian technique should actually be more reliable. Finally, small differences can be caused by the turbulence scheme in FLEXPART, whose horizontal components affect $E - P$ diagnostics as particles move from one grid cell to another; $E - P$ estimates should actually be improved by the turbulence scheme, but this is hard to verify.

The differences between the forecasts and both diagnostic methods are much larger. For instance, in the forecasts the precipitation surplus in most of the ITCZ, especially over the Indian and Pacific Oceans, is larger than that obtained with the diagnostic methods, and there is also more precipitation at the entrance to the North Atlantic storm track. Both appear to be linked with the ECMWF model's convection scheme. Globally averaged, the annual freshwater flux is -145 mm for the forecasts, but less than 1 mm for both diagnostic methods. Unbalanced moisture fluxes are a well-known problem when using forecast data because moisture can unphysically be introduced into or removed from the model by the data assimilation (Trenberth 1997). Because of model spinup, forecast fluxes also depend on the forecast lead time, causing additional ambiguities. In contrast, both diagnostic methods are almost exactly balanced globally for long-term averages, for which the tendency term in (1) vanishes. The correlation between Lagrangian and forecast $E - P$ estimates ($r^2 = 0.86$; see Fig. 3b) is in fact higher than the correlation between Eulerian and forecast $E - P$ estimates ($r^2 = 0.80$), perhaps pointing to a higher accuracy of the Lagrangian method.

Figure 4 shows annual P from 24-h forecasts, the Lagrangian technique, and the GPCP observations. All three datasets show the same global patterns, but also differ quite significantly from each other. The forecasts underestimate P over the Sahara and overestimate P over most of the rest of the globe (especially in the Arctic and ITCZ) relative to the GPCP data. The Lagrangian method gives relatively good results in regions of high precipitation, that is, in the ITCZ and in the midlatitude storm tracks, but it severely overestimates P in regions where P is small, especially in the subtropics. This positive bias at low values can best be seen in the scatterplots shown in Figs. 3c and 3d. Much of this bias may be due to condensation–evaporation cycles of cloud droplets, leading to false diagnosis of P in one

←

FIG. 2. The quantity $E - P$ derived from (a) ECMWF 24-h forecasts, (b) the Eulerian diagnostic based on ECMWF analyses, and (c) the Lagrangian diagnostic based on ECMWF analyses, for the year 2000.

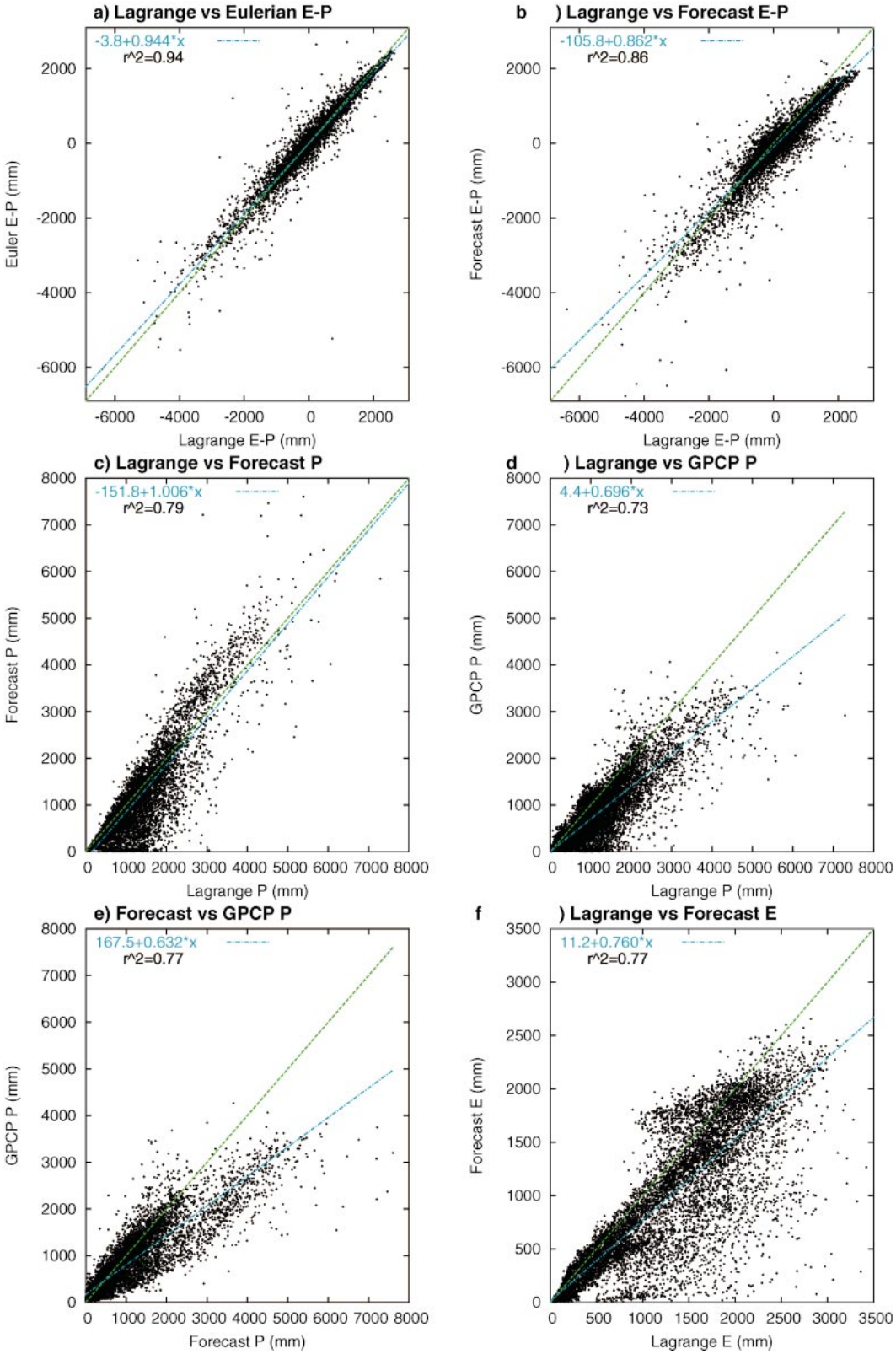

FIG. 3. Correlations between (a) Lagrangian and Eulerian $E - P$, (b) Lagrangian and forecast $E - P$, (c) Lagrangian and forecast P, (d) Lagrangian and GPCP P, (e) forecast and GPCP P, and (f) Lagrangian and forecast E. Dashed lines show $y = x$; dash–dot lines are linear fits shown in the upper left corner of each panel; and r^2 is the variance explained by the fit.

and of E in a later time step, as discussed in section 2. In the future this could be taken into account by adding the liquid and ice water content to q. However, because trajectories also contain calculation errors, some of the q fluctuations along them may be entirely unphysical (Stohl and Seibert 1998).

In regions where P is large, the Lagrangian method shows a good skill, especially compared to P forecasts (Fig. 3c). Compared to the GPCP data there seems to be a significant positive bias even for the largest P values (Fig. 3d), but this bias is even more severe for the forecast P (Fig. 3e). A comparison with independent rain gauge measurements indeed revealed that GPCP is biased low by 16% on average and more for large P values in the Pacific (Adler et al. 2003). Generally, it seems that the air masses producing strong precipitation can be successfully identified based on the particle information alone. This in turn allows their transport histories to be studied, which is the ultimate aim of the Lagrangian method.

Figure 5 shows annual evaporation from 24-h forecasts and the Lagrangian diagnostic. The large-scale patterns in the two fields agree well, but the Lagrangian method overestimates E, as also seen in Fig. 3f, because of the problems discussed earlier. This is most severe in the Sahara, where evaporation rates are unrealistically high. Globally averaged, $E = 1080$ mm for the forecasts, but $E = 1380$ mm for the Lagrangian method. However, some rather small-scale patterns are well diagnosed, like the high evaporation rates over the Red Sea or at the eastern seaboard of North America, and a linear fit between forecast and Lagrangian E estimates explains 77% of the variance.

b. Case study of a heavy precipitation event

For a regional case study, we have chosen the heavy precipitation event that led to severe flooding in large parts of central Europe in August 2002. On 12 August 2002, the largest 24-h accumulated precipitation, 352.7 mm, ever recorded in Germany fell over the station Zinnwald-Georgenfeld, and more than 150 mm fell over a widespread area (Rudolf and Rapp 2003). Some regions were already inundated before this event from another severe precipitation event that had occurred just the week before. Moreover, soils in large regions of Europe were saturated from a wet spell in July (James et al. 2004). Altogether this led to floods with return periods of 100 to 300 yr in several large river catchments, most catastrophic in that of the Elbe. Weather forecast models predicted heavy rain a few days in advance, but underestimated the severity of the event (Rudolf and Rapp 2003; Grazzini and van der Grijn 2003). For an evaluation of the ECMWF forecasts for this episode see Grazzini and van der Grijn (2003); for a synoptic description of the episode see Ulbrich et al. (2003a,b) and James et al. (2004, manuscript submitted to *Quart. J. Roy. Meteor. Soc.*), who also used a simple trajectory model to study water vapor transport. Mean sea level pressure maps from 10 to 12 August (Fig. 6) show the development of a low over the Ligurian Sea on 10 August, whose center traveled to the Adriatic Sea on 11 August and subsequently moved northward to central Europe. This classical Vb cyclone track (van Bebber 1891) has a reputation for causing heavy rain over central Europe. The development was favored by an upper-level trough (not shown) over the United Kingdom 9 August, which spawned a cutoff low over the Mediterranean on 11 August.

ECMWF analysis data with a resolution of 1° for the entire globe, and 0.5°-resolution data for the region 18° to 66°N and 105°W to 45°E were available. FLEXPART was run for a domain from 28° to 65°N and from 25°W to 55°E for the period from 27 July to 14 August. Particles were created and destroyed at the domain boundaries. About 2.8 million particles were present in the computation domain at any time. Sets of 6- and 24-h E and P forecasts were used for comparison. As these two sets were relatively similar, we only show the 6-h forecasts.

Figure 7 shows P from the ECMWF forecasts and the Lagrangian diagnostic, and Fig. 8 shows GPCP data and gridded rain gauge observations for the period 10–13 August 2003. The gauge data were available only from synoptic stations and were gridded using the algorithm used by the Global Precipitation Climatology Centre (Rudolf et al. 2003). The dataset does not include some of the most extreme observations of rain amount made at nonsynoptic stations. The maximum P values (at 1° resolution) were 134, 121, 108, and 110 mm for the forecasts, the Lagrangian diagnostic, the GPCP data, and the gridded gauge data, respectively. As discussed before, the Lagrangian diagnostic (Fig. 7b) overestimates the precipitation, especially where it is low, because of relatively high levels of noise. Generally, however, P features are in relatively good agreement with the other datasets. In fact, some structures in the diagnosed P field are perhaps in better agreement with the gauge measurements, particularly those from the high-resolution network shown in Rudolf and Rapp (2003), than both the forecasts and the GPCP data. The double maximum of P over eastern Germany is absent in the forecasts and the GPCP data but, depending on contouring, can be seen in the gauge data. Particularly, it is confirmed by maps based on a more complete rain gauge dataset (Rudolf and Rapp 2003) showing a second P maximum north of 50°N, which was actually caused by orographic effects. There was also indeed strong precipitation west of the Caspian Sea on 10 and 11 August, which is missing in the GPCP data and only hinted at in the ECMWF forecasts.

Figure 9 shows E from ECMWF forecasts and the Lagrangian method. In the forecasts, the evaporation patterns are relatively simple: There are two maxima over the western Mediterranean and over the Caspian Sea, very low values over Africa, and small values else-

a) P from ECMWF forecast

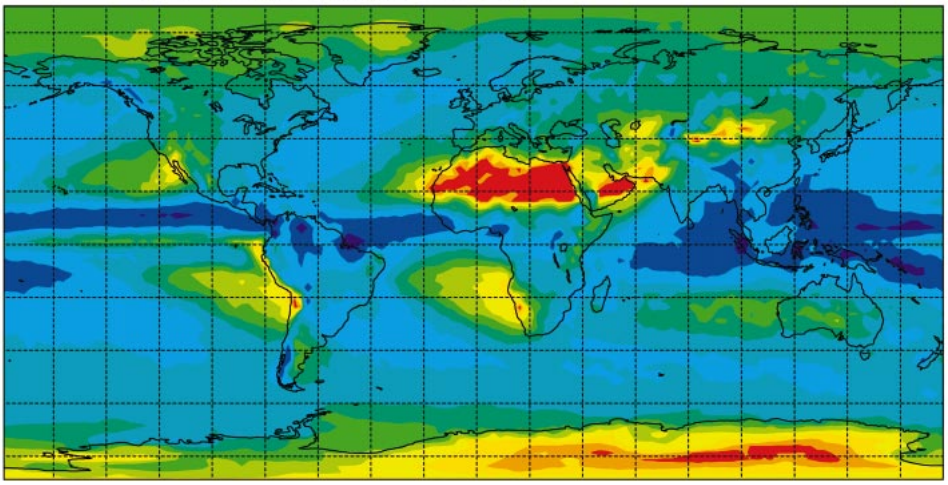

b) P from Lagrangian diagnostic

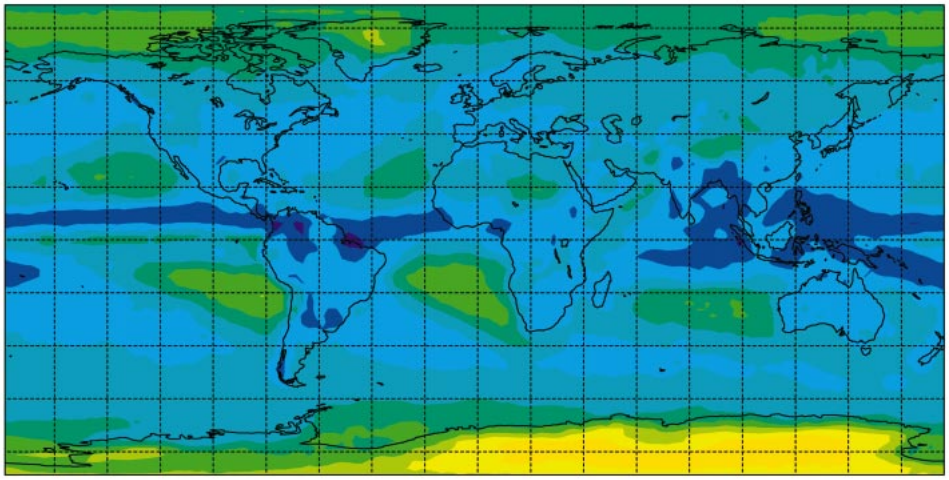

c) P from GPCP observations

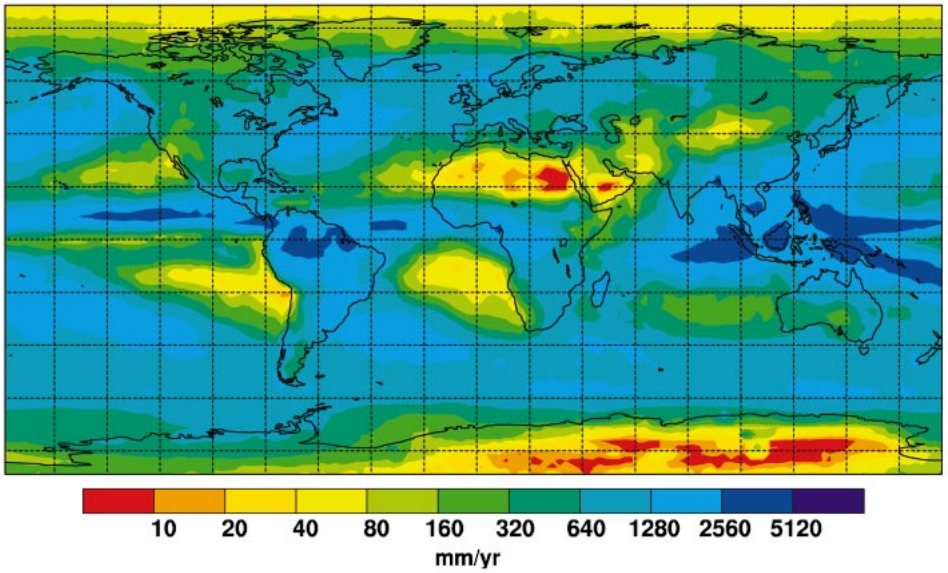

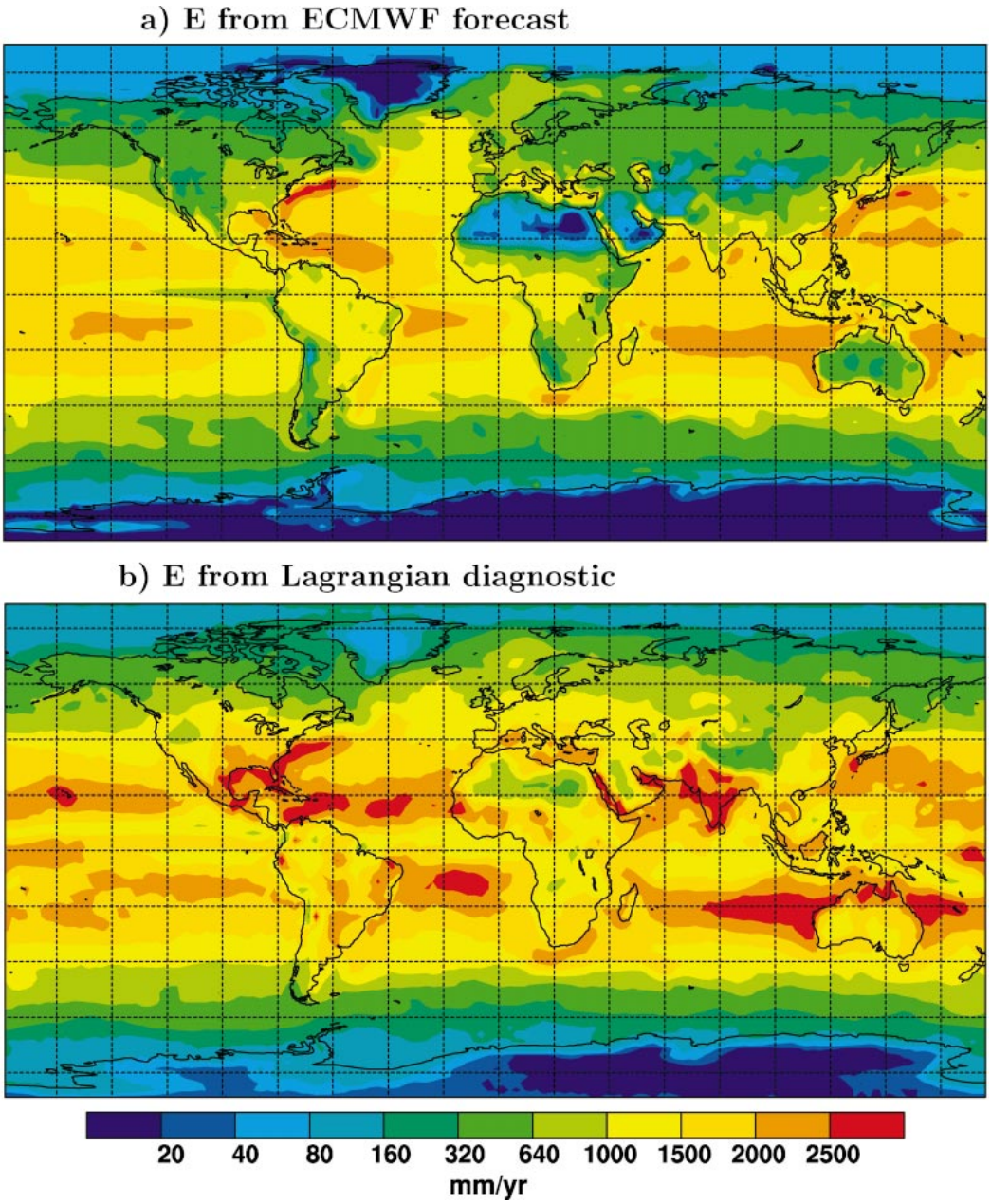

FIG. 5. Evaporation *E* derived from (a) ECMWF 24-h forecasts, and (b) the Lagrangian diagnostic based on ECMWF analyses, for the year 2000.

where. The Lagrangian method, in contrast, shows very complicated patterns over a noisy background: In addition to the maxima over the western Mediterranean (which extends farther east than in the forecasts) and the Caspian Sea, relatively high values are also found over northern Algeria, the Black Sea, and the Ukraine. Lacking representative observations of *E,* it is hard to tell whether these maxima are realistic or not. However, there are indications that some may indeed be correct. The days before 10 August experienced heavy rain in large areas of central and eastern Europe. Parts of eastern Austria were inundated, due to heavy rain on 6 and

←

FIG. 4. Precipitation *P* derived from (a) ECMWF 24-h forecasts, (b) the Lagrangian diagnostic based on ECMWF analyses, and (c) GPCP observations, for the year 2000.

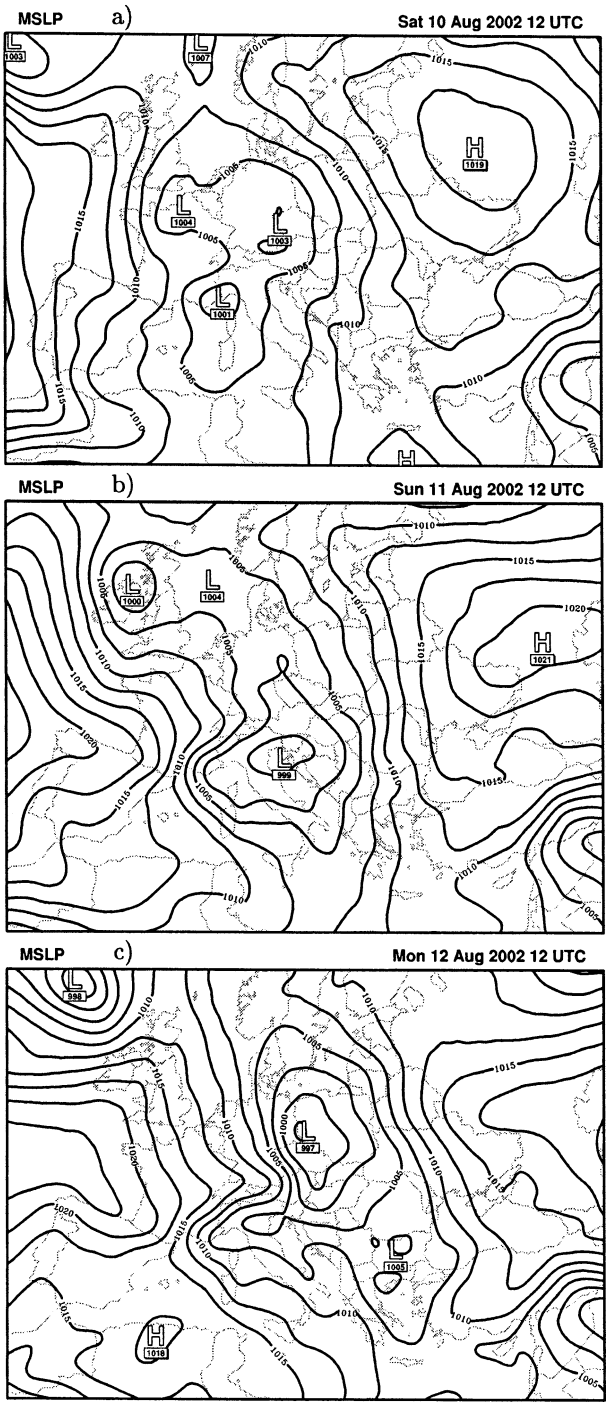

FIG. 6. Maps of mean sea level surface pressure on (a) 10, (b) 11, and (c) 12 Aug 2002 at 1200 UTC. Isolines are drawn every 2.5 hPa.

7 August. Despite sunny weather between the two rain episodes, forecast evaporation fluxes were only about 2 mm day^{-1} in this region. According to the GPCP data some rain fell in northern Algeria the week before, where ECMWF predicted much less than 1 mm of evaporation over the 4-day period. Based on ECMWF reanalysis data, James et al. (2004, manuscript submitted to *Quart. J. Roy. Meteor. Soc.*) found that on a 1 million km^2 space and 7-day time scale, the third largest precipitation event over Europe since 1958 occurred in southern Europe just 3 weeks before the event discussed here (which classified as the largest one). The GPCP data show that the entire second half of July was extremely wet in large parts of Europe, particularly in southern Europe (southern France, Italy, and Greece) and the Ukraine. It is remarkable that the Lagrangian method diagnoses large E values in exactly these regions. In contrast, it seems that the land surface scheme of the ECMWF model could not handle the water from these previous precipitation events well enough and underestimated evaporation. Underpredictions of the heavy rain, particularly for longer forecast times, may have been the consequence.

Figure 10 shows $E - P$ from the forecasts, the Eulerian method, and the Lagrangian method (note that Fig. 10b shows an area shifted to the west by 10° compared to Figs. 10a and 10c, because the Eulerian method could be used only over the nested domain). All three methods show $E - P < 0$ over central Europe. However, while the forecasts suggest $E - P > 0$ over most other regions, both diagnostic methods show much higher spatial variability, which may or may not be realistic. Diagnosed $E - P$ is much larger than forecast $E - P$ over many land surfaces, again suggesting that the ECMWF forecasts underpredicted evaporation. The agreement between the two diagnostic methods is less good than in the global study. However, this was expected, as here also some details of the numerical implementation become important in addition to the differences noted in the previous section. The Lagrangian technique diagnoses $E - P$ between two time steps, whereas the Eulerian technique diagnoses it at a particular time using previous and subsequent fields for diagnosing term 1 on the right-hand side of (1). This leads to incorporation of slightly different data by the two methods at the beginning and at the end. While this can be neglected for an entire year, it is of significance for a four day period. Given these differences, we again find a very good general agreement between the two methods.

4. Results: Demonstration of moisture tracking

Many scholars (e.g., Smirnov and Moore 2001; Liu and Stewart 2003) have studied the source regions of water vapor using maps of the vertically integrated moisture flux $\mathbf{Q} = 1/g \int_0^{p_s} q\,\mathbf{v}\,dp$. Figure 11 shows $\mathbf{Q}$, vectors coded with a color scale for $E - P$ from the Eulerian method, for three subsequent days of the 2002 event. Particularly on the second day (1200 UTC 11 August to 1200 UTC 12 August) large moisture fluxes originate southwest of the cyclone's center over a strong evaporative source region in the Mediterranean. The moisture then spirals around the cyclone into the region

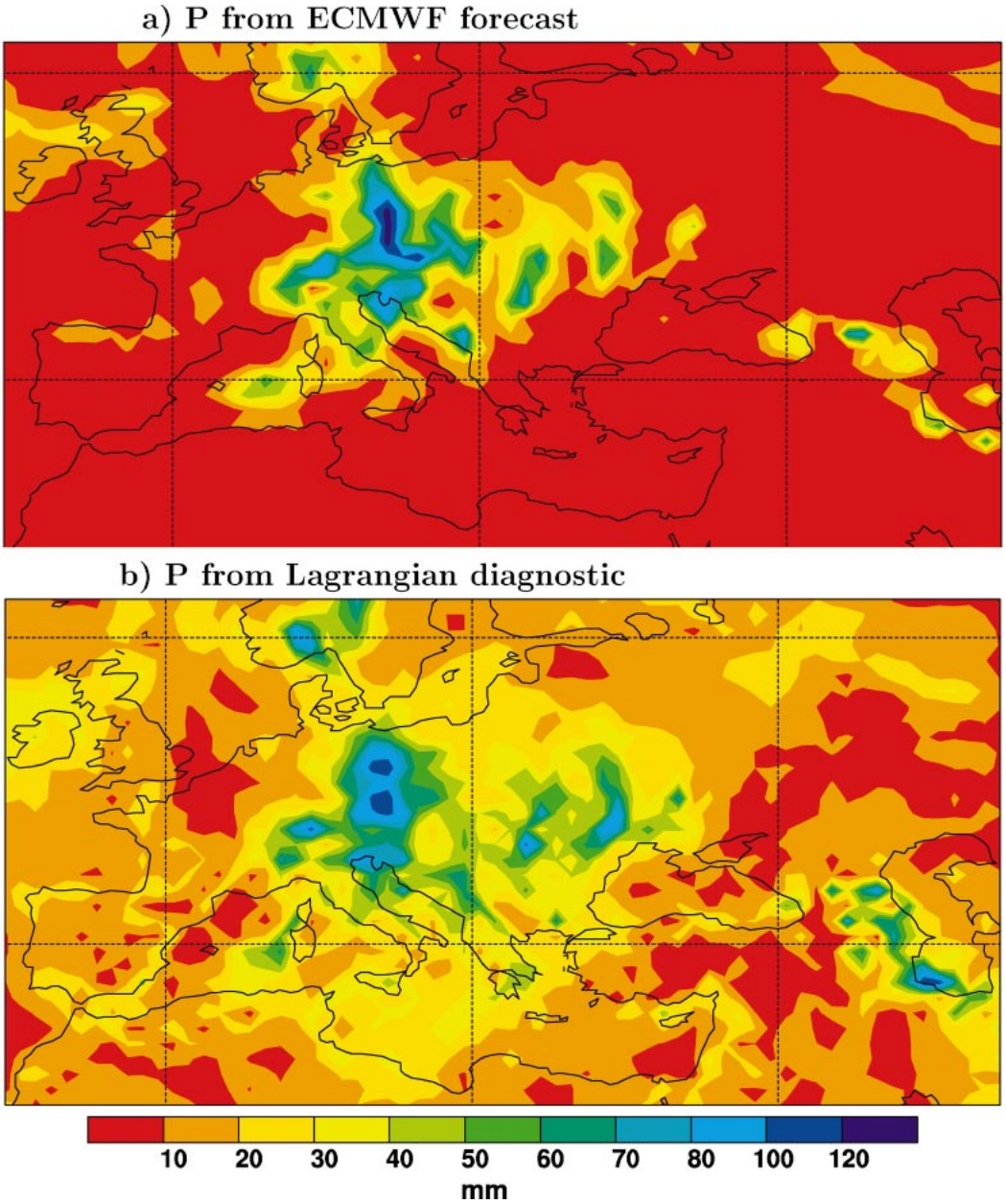

FIG. 7. Precipitation *P* derived from (a) ECMWF and 6-h forecasts, and (b) the Lagrangian diagnostic based on ECMWF analyses for the period 10–13 Aug 2002.

of strong precipitation. This suggests a relatively simple source–sink relationship with water sourced from the western Mediterranean being rained out over central Europe. However, the sequence of **Q** maps shows considerable variability. Particularly on the third day, when the cyclone has traveled farther east, there are also relatively large moisture fluxes over the Black Sea and continental eastern Europe. But whether they contribute to the precipitation in central Europe or not is unclear. Because of the nonstationarity of the wind and **Q** fields, causing large differences between trajectories and streamlines, it can be misleading to establish source–receptor relationships based on **Q** fields.

To demonstrate the capacity of the new method for identifying the moisture source regions, we first need to define the precipitation event in space and time. For this, four criteria were applied: First, the period was chosen as 10–13 August, which encompasses the entire event. Second, the target area was selected as ranging from 43° to 54°N and 8° to 19°E. Like the first criterion, this definition is generous (cf. Fig. 7b), but it excludes rain not associated with the low that produced the flood-

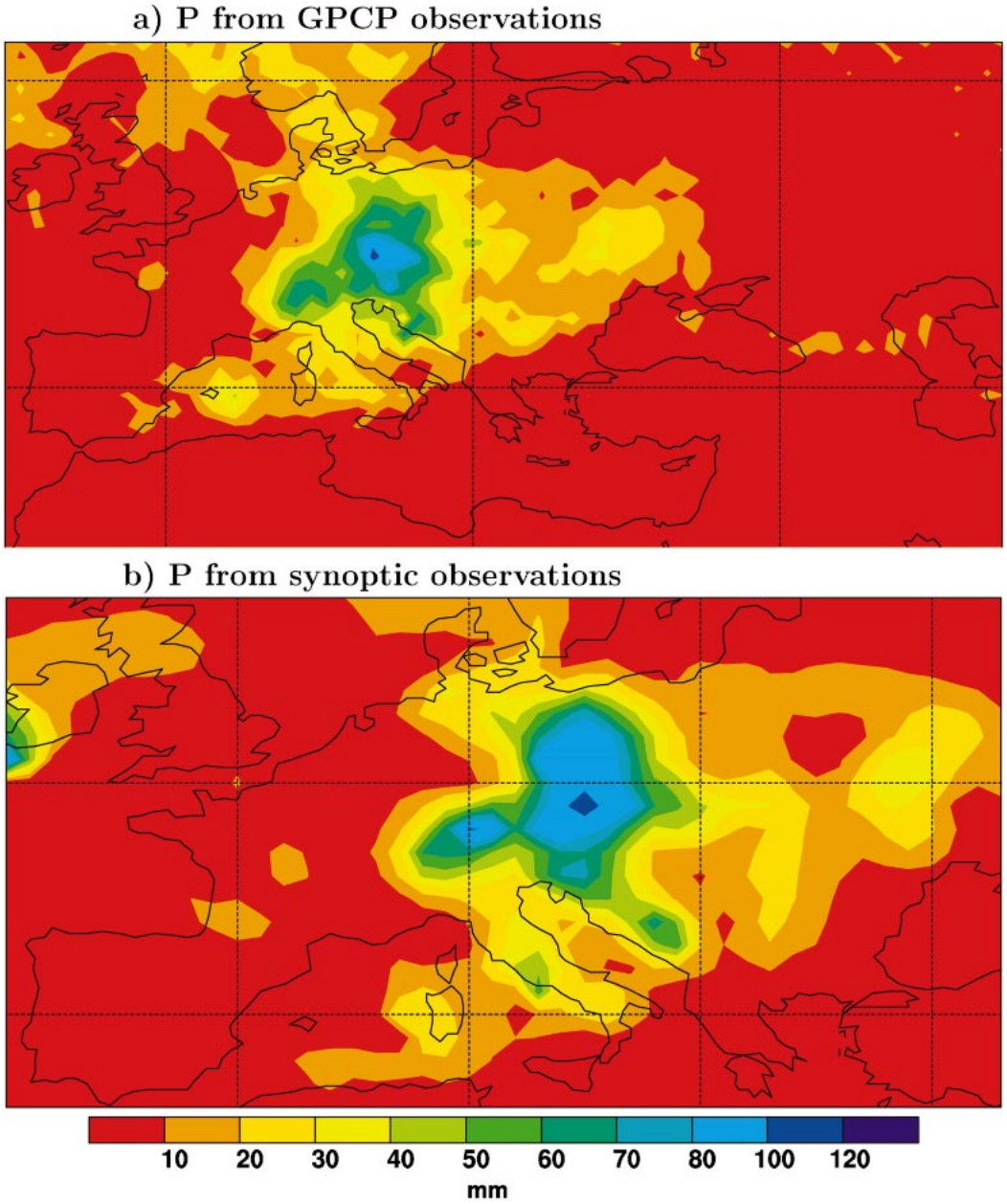

FIG. 8. Precipitation P from (a) the GPCP daily dataset for the period 10–13 Aug 2002, and (b) gridded rain gauge observations from synoptic stations for the period from 0600 UTC 10 Aug to 0600 UTC 14 Aug.

ing. Third, we only considered grid cells where, and the times when, the Lagrangian method diagnosed $E - P < -2$ mm h^{-1} (note that instantaneously $E - P = -P_i$). This is a subjective threshold that shall include most of the precipitation, while reliably excluding regions and periods without significant rainfall. Fourth, we only considered particles with $e - p < 0$ during a time step fulfilling the other three criteria. This criterion served to further narrow down the air masses that actually produced the rain, both horizontally and vertically. Figure 12 shows P obtained with the Lagrangian method as applied in section 3, but only for the particles fulfilling the above criteria. A comparison with Fig. 7b reveals that the distribution of P within the target area is well preserved, but precipitation maxima are slightly reduced because periods of light rain have been excluded.

The particles selected by the above criteria were traced back in time for 10 days. Figure 13 shows the trajectories 6 days back in time for randomly chosen 1% of the particles fulfilling the target criteria at three different 1-h periods. On 11 August, trajectories end mainly in the southernmost part of the target region.

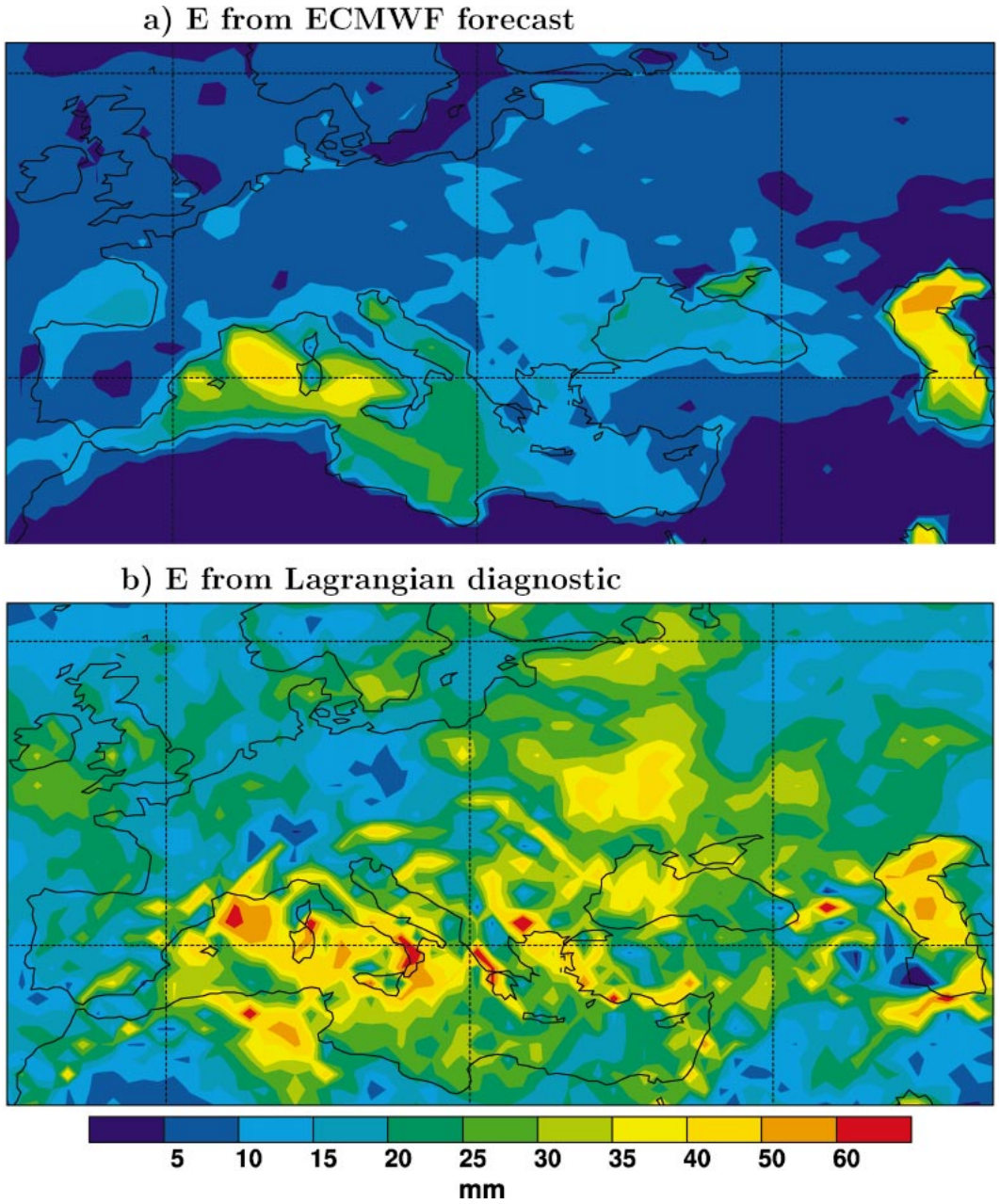

FIG. 9. Evaporation *E* derived from (a) ECMWF 6-h forecasts, and (b) the Lagrangian diagnostic based on ECMWF analyses, for the period 10–13 Aug 2002.

One day later, their end points have shifted farther north, and on 13 August trajectories only end in a relatively small region in the northeast of the target domain, indicating the shift in rainfall patterns. The trajectories are colored according to dq/dt in order to show regions of water vapor gain and loss. Upon arrival in the target region all particles per definition lost water vapor, whereas before, there are both trajectory segments where water was lost and such where it was gained. This occurred partly in the same regions, which can be explained both by differences in altitudes and times when they traveled over a certain location.

On the first day, 11 August at 0000 UTC (Fig. 13a), most of the trajectories arrived from the North Atlantic and made their final approach to the target region over the Mediterranean, where many of them gained substantial amounts of moisture. However, there were also other pathways: A swarm of particles, whose origin in Fig. 13a is over the North Sea, was still over Europe 10 days back. Some particles also arrived from North

a) E - P from ECMWF forecast

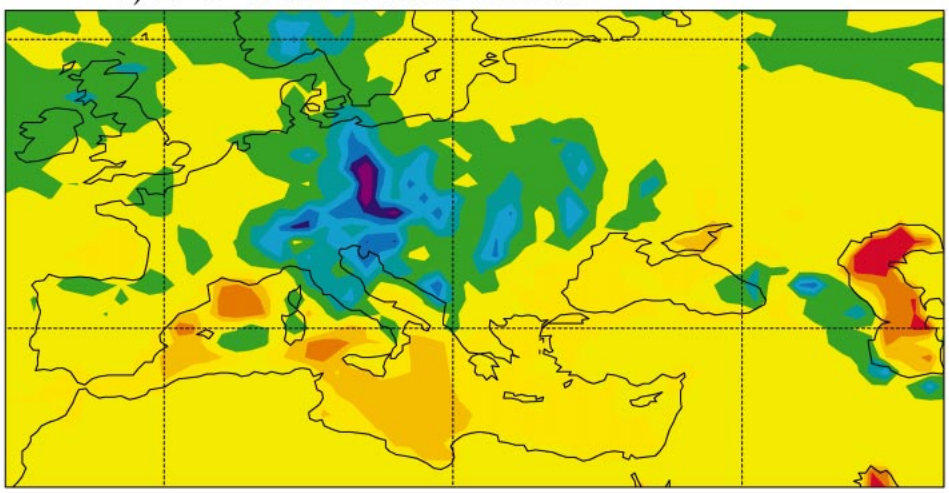

b) E - P from Eulerian diagnostic

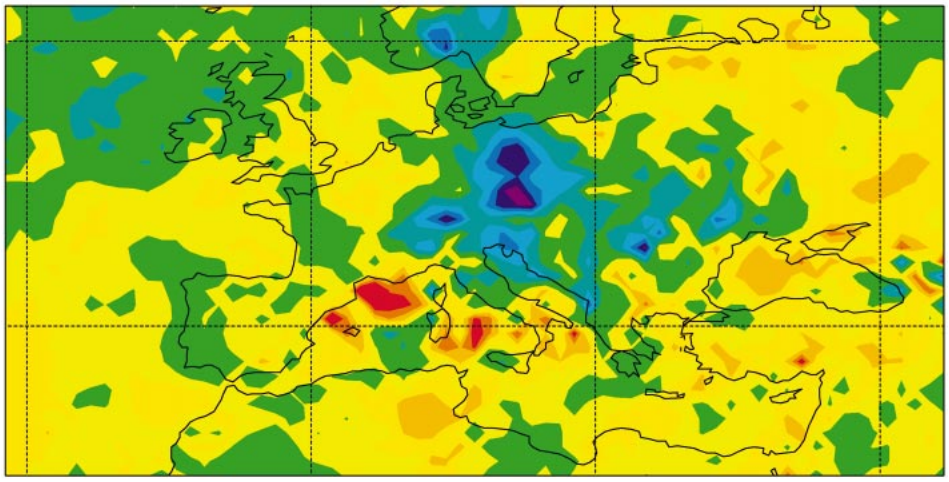

c) E - P from Lagrangian diagnostic

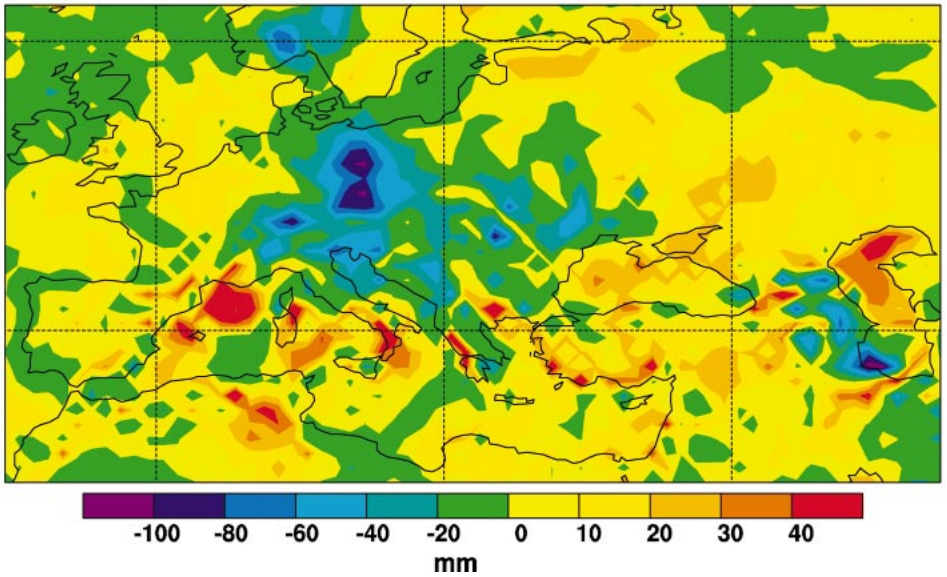

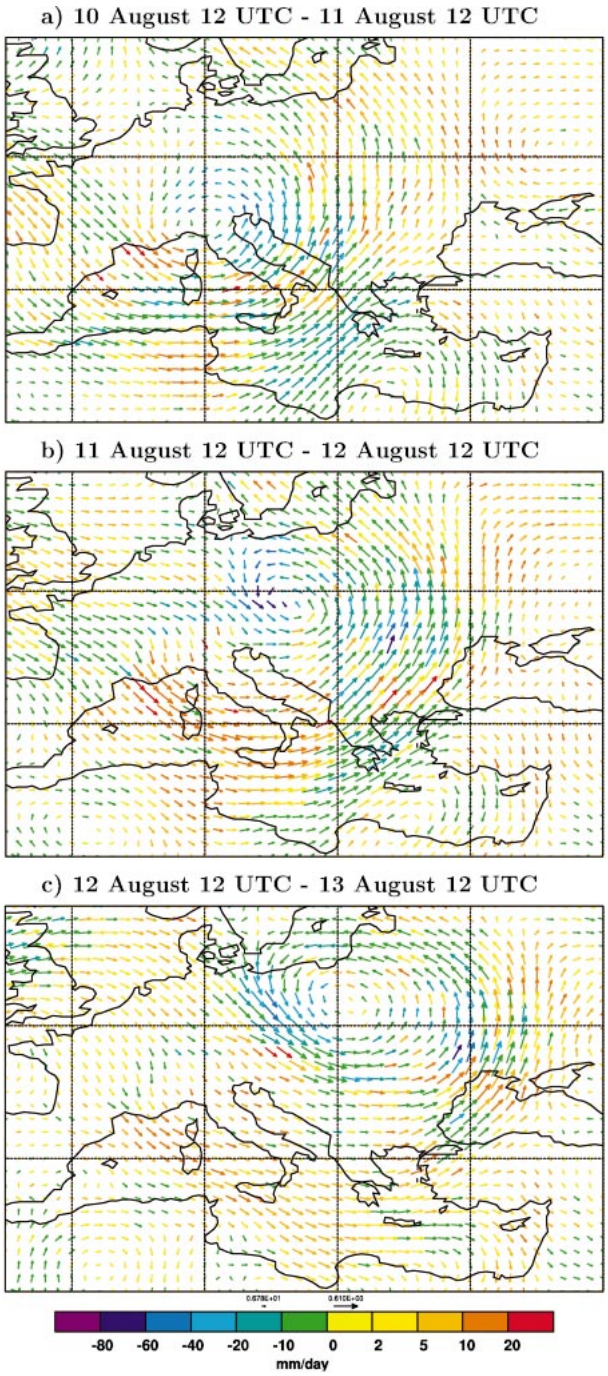

FIG. 11. The 24-h average vertically integrated water vapor fluxes **Q** (kg m^{-1} s^{-1}) for (a) 1200 UTC 10 Aug to 1200 UTC 11 Aug, (b) 1200 UTC 11 Aug to 1200 UTC 12 Aug, and (c) 1200 UTC 12 Aug to 1200 UTC 13 Aug. The maximum vector length is 610 kg m^{-1} s^{-1}. Vectors are represented according to the color scale for $E - P$.

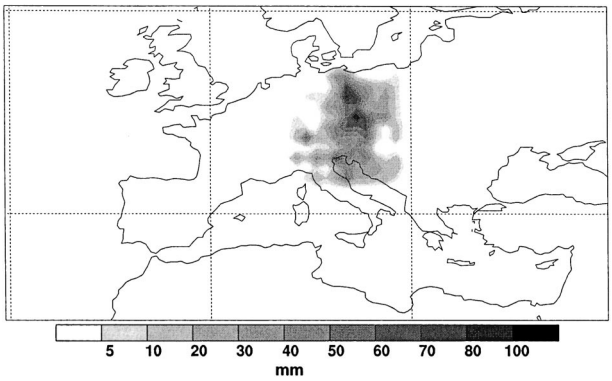

FIG. 12. Target precipitation as obtained with the Lagrangian method. The target criteria are explained in the text.

Africa. These originally very dry particles received substantial moisture over Algeria and the Mediterranean. And finally, some particles also arrived from the east, traveling mostly over land.

One day later (Fig. 13b), particles did not arrive in the target region directly from the Mediterranean, but spiralled around the eastern edge of the cyclone toward its center (cf. Fig. 11b), thereby crossing large land areas (e.g., northern Greece), where their moisture increased dramatically. Furthermore, a relatively large number of particles also arrived directly from Asia. On 13 August (Fig. 13c), the particles spent even more time over land. Some particles also crossed the northern part of the Black Sea, where their water vapor content increased strongly. The flood-producing cyclone obviously incorporated precipitating air masses of vastly different origins in its circulation. All these air masses finally converged and spiralled cyclonically into the target area.

While the trajectory plots show the pathways of the precipitating air masses and also indicate some regions where they have likely sourced water, these plots are relatively qualitative, valid for particular 1-h periods only, and show a small percentage of the particles that produced the rain. Therefore, we gridded the trajectory information onto a $1° \times 1°$ grid, using all particles and for the full 10-day trajectory length. Figure 14 shows the time particles have spent in the grid cells during the 10 days before arrival in the target region, weighted with the precipitation rate upon arrival. Figure 14a shows the residence times in the total atmospheric column, whereas Fig. 14b shows the residence times only in the PBL. The residence times for the full columns (Fig. 14a) are in good agreement with the qualitative trajectory information shown in Fig. 13, summarizing all the major pathways. However, because water vapor sources are ultimately located at the surface, the resi-

←

FIG. 10. The quantity $E - P$ derived from (a) ECMWF 6-h forecasts, (b) the Eulerian diagnostic based on ECMWF analyses, and (c) the Lagrangian diagnostic based on ECMWF analyses, for the period 10–13 Aug 2002. The domain for the Eulerian method is shifted by 10° to the west relative to the other two domains, because no data with 0.5° resolution were available east of 45°E.

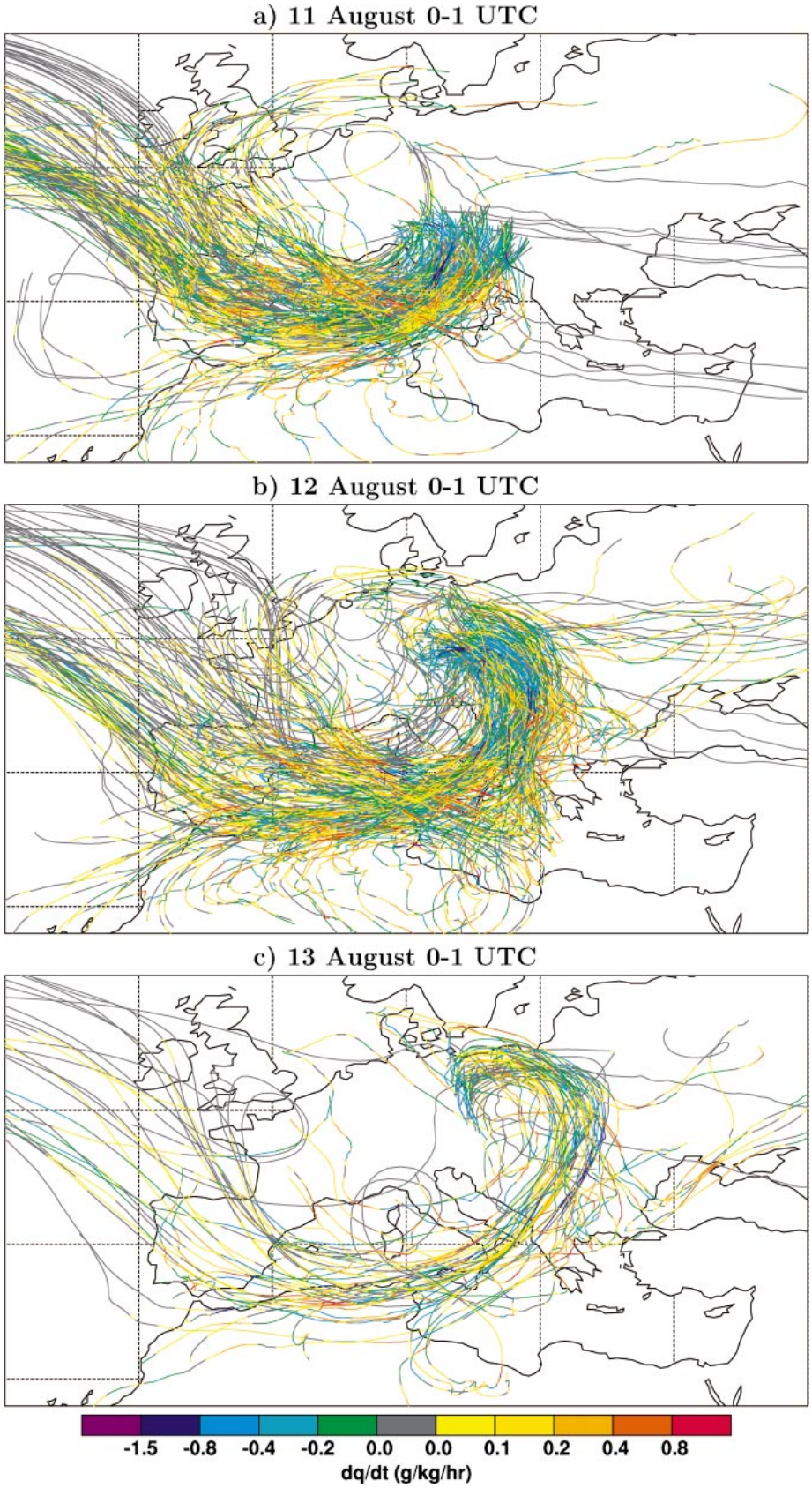
a) 11 August 0-1 UTC
b) 12 August 0-1 UTC
c) 13 August 0-1 UTC
-1.5 -0.8 -0.4 -0.2 0.0 0.0 0.1 0.2 0.4 0.8
dq/dt (g/kg/hr)

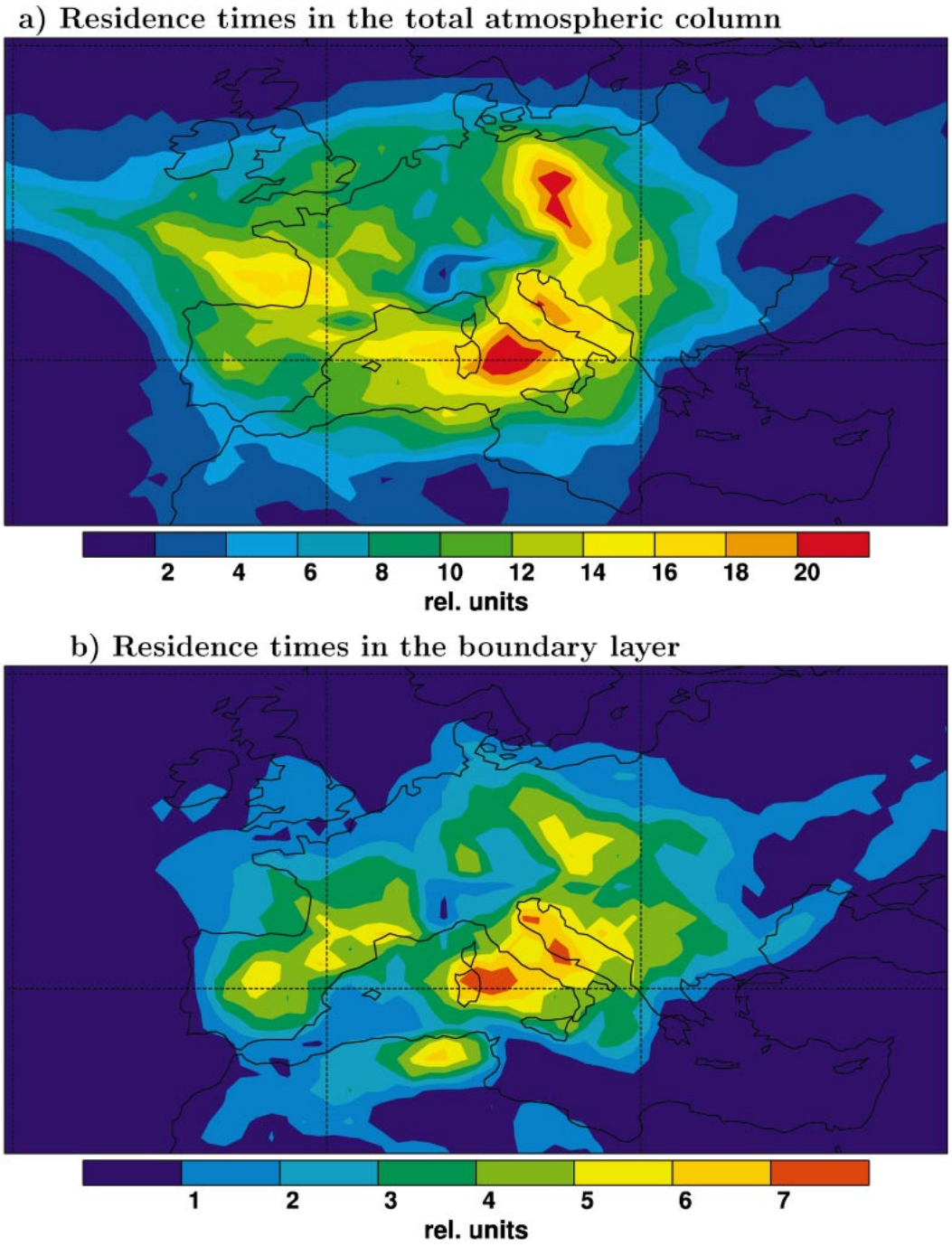

FIG. 14. Residence times of particles in columns of the output grid, weighted by their target precipitation, during the 10 days preceding the time step when the target criteria were fulfilled in (a) the total atmospheric column, and (b) only in the PBL. The same relative units were used in both (a) and (b).

←

FIG. 13. The 6-day back trajectories of particles fulfilling the target criteria in the hour from 0000–1000 UTC for (a) 11 Aug, (b) 12 Aug, and (c) 13 Aug. The trajectories are colored according to the gray scale for moisture changes dq/dt. For clarity, dq/dt values were smoothed over 6 h and absolute values less than 0.02 g kg^{-1} h^{-1} were set to 0. Trajectories are shown only for randomly chosen 1% of the target particles.

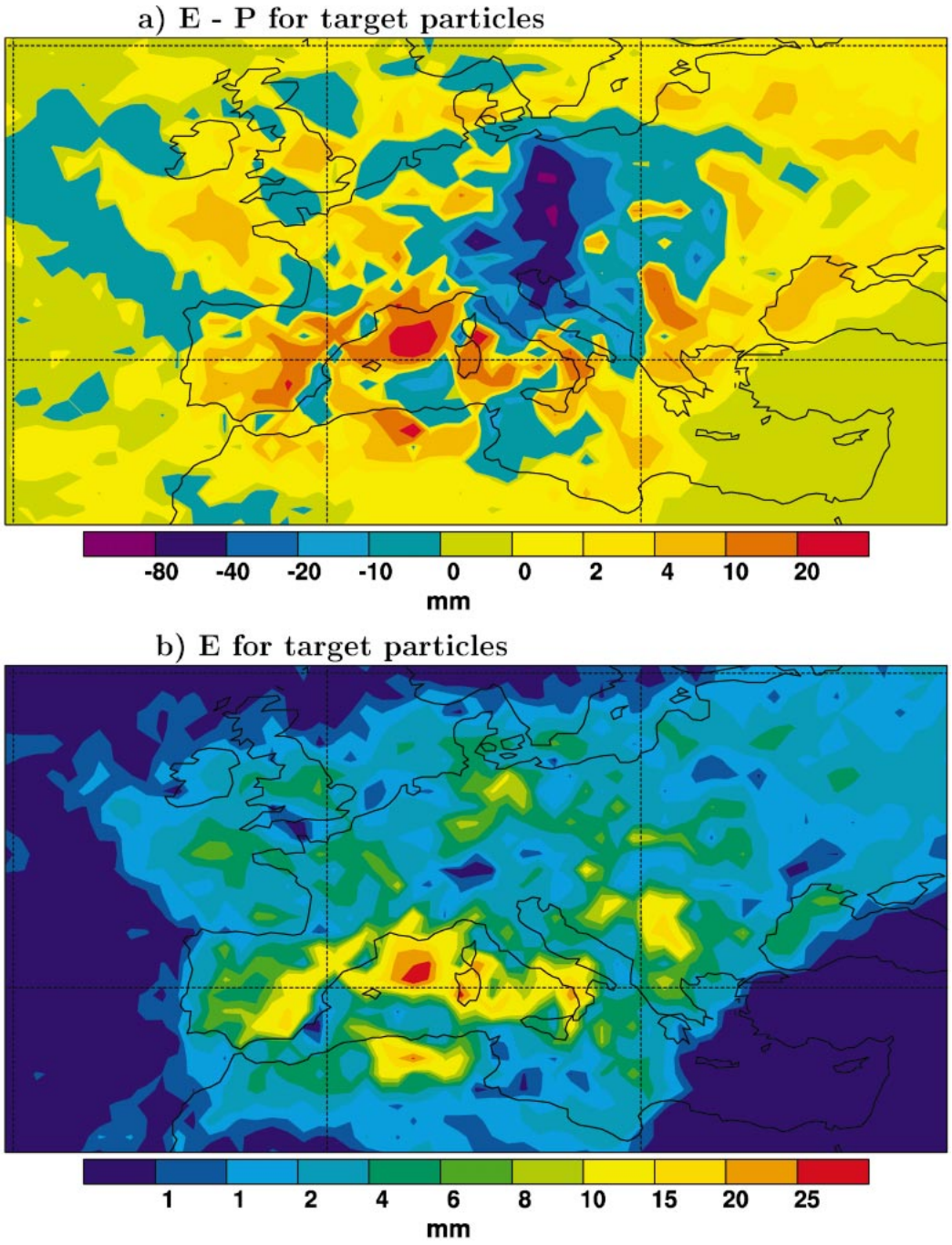

FIG. 15. (a) The quantity $E - P$ and (b) E for target particles during the 10 days preceding the time step when the target criteria were fulfilled. The greenish color in (a) extends from −0.4 to 0.1 mm and mostly demarcates areas with very low densities or absence of particles (e.g., the southeast corner of the plot).

dence times in the PBL (Fig. 14b) are more interesting. The longest residence times in the PBL are found in the Adriatic and Tyrrhenian Seas, but relatively long residence times are also seen over Spain and southern France, northern Algeria, and to the east of the target area.

The PBL residence times indicate where evaporation may have been important, but they do not give quantitative information on evaporation. In the absence of evapotranspiration, even a long PBL residence time will not lead to moistening. Therefore, we again apply the Lagrangian budget approach to diagnose $E - P$, but this time using only the target particles. Figure 15a shows $E - P$ accumulated over the 10 days prior to the

target time and for the target particles only. The $E - P$ distribution reveals where the particles participating in the rain event took up and where they lost moisture. Here, $E - P$ is negative over the target region, but smaller negative values can also be found over other regions of Europe. This indicates that some of the particles already produced precipitation before reaching the target. The precipitation over the Mediterranean was associated with the same cyclone that caused the flooding, whereas the precipitation over the Atlantic marks the path of a patch of particles arriving from the Atlantic storm track only about 2 days before reaching the target region. As expected, target particles experienced net evaporation over large regions of the Mediterranean. These regions correspond to where many particles touched down into the PBL (cf. Fig. 14b), but the patterns are strongly modified by the local moisture budget. For instance, the PBL residence times (Fig. 14b) show a relatively minor pathway over the Black Sea, but particles nevertheless took up much moisture there because of the high evaporation rates (Fig. 9). While the strong contribution of evaporation over the Mediterranean was expected for this type of meteorological situation, it is perhaps surprising to see how large areas actually fed moisture into the flood-producing cyclone.

Calculating E for the target particles only is even more problematic than for the full set of particles. As particles disperse back in time, fewer and fewer particles are found in any particular grid column. This means that there is less chance for cancellation between particles of noise in the $e - p$ values, which also makes instantaneous $E - P$ values more noisy. According to our definition, more noisy instantaneous $E - P$ values lead to overestimates of both E_i and P_i. The distribution of accumulated E for the target particles (Fig. 15b), thus, must be interpreted with caution. However, the maxima in E are consistent with those found for $E - P$ and likely mark the true main source regions of the water vapor that became precipitation.

The E distribution for target particles suggests that evaporation both from land and sea has contributed to the flooding event. The single largest source region was the western Mediterranean, with smaller contributions coming also from other oceanic regions: the North Atlantic, the Baltic Sea, and the Black Sea, which all had positive sea surface temperature anomalies compared to the climate-mean conditions for this time of the year. Another E maximum is found over Yugoslavia and Bulgaria, a region that, according to GPCP data, received about 40 mm of rain from 2 to 9 August, most of which fell on 7 and 8 August and was associated with the same cyclone that caused the flash floods in northeastern Austria on 7 August. This region also received some 80 mm of rain during the second half of July. The same is true for the scattered E maxima in eastern Europe and northern Germany, where about 50 mm of rain fell from 2 to 9 August, and much more in July. This clearly shows how important the previous heavy rain was for providing extra water that otherwise would not have been available for evaporation. Precipitation recycling over land, thus, seems to have been a major contributing factor to the severe flooding.

There were only about 10 mm of rain over Algeria and southeastern Spain, and somewhat more in northeastern Spain, from 2 to 9 August. Eastern Spain and southern France also received 20–80 mm, and Algeria some 5–10 mm, during the second half of July, according to the GPCP data. Partly, the large water contribution from these regions are due to the long time that target particles have spent in the PBL over these regions (see Fig. 14b). Evaporation, nevertheless, must have been active in these relatively arid regions if the $E - P$ budgets (and, thus, the ECMWF analyses) are correct. However, there is also the possibility that evaporating hydrometeors may have been the source of the moisture. While $E - P$ diagnosed in a column with equally distributed particles (as in section 3) must be balanced by the surface freshwater flux, this is not necessarily true for the target particles only because they do not occupy the whole atmospheric column. In that case, $E - P$ may also be positive when hydrometeors from a nontarget (and thus not accounted for) overhead air mass fall into and evaporate in the target air mass. This may indeed have occurred, at least over Spain.

Some scholars (e.g., Eltahir and Bras 1996; Trenberth 1999) have calculated precipitation recycling ratios to characterize how much moisture that precipitates out at a particular location comes from local evaporation. There exist different definitions for the recycling ratio, which are all dependent on a length scale. An analog to the recycling ratio based on our results is the fraction of the target precipitation that has evaporated in the target domain itself (an area of roughly 900 km $\times$ 1200 km) during the previous 10 days. Alternatively, a suitably defined different domain or a different time period could also be used. We find that of the 24 gigatons (Gt) of target precipitation, 9 Gt evaporated in the target region itself during the previous 10 days (i.e., a recycling ratio of 37%), and 22 Gt in a larger domain from 40° to 60°N and 0° to 20°E. However, one difficulty with the estimate of a recycling ratio is that our E values are biased high, as mentioned before. Recycling ratios must, therefore, be considered as upper estimates only. Note also that local recycling (i.e., coexistence of E and P in a grid cell at the same time) is excluded in our calculation of E. The advantage, on the other hand, is that one is not restricted to the calculation of a local recycling ratio, but can calculate the contribution of any region to the target precipitation.

Another interesting aspect of our method is to investigate when the water that became precipitation evaporated. Figure 16 shows the temporal evolution of E, P, and $E - P$, accumulated over all target particles from the target time (0) back over the previous 10 days. Accumulated $E - P$ drops from 0 to -24 Gt within one time step from target time, because of the selected heavy

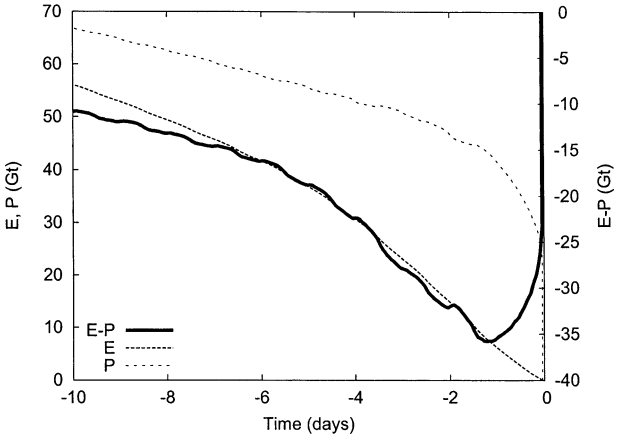

FIG. 16. Time evolution of $E - P$ (solid line), E (short-dashed line), and P (long-dashed line) in Gt of water, accumulated over the 10 days preceding the time step when the target criteria were fulfilled.

precipitation. At this time step, $E - P = -P_i$ because only precipitating particles were considered. Accumulated P continues to rise because not all the precipitation did fulfill the target criteria (i.e., it fell outside the target area, before 10 August, or was too light). After about 1 day, however, when most particles have left the precipitating cloud system, the rise in accumulated P slows down. Also after circa 1 day, $E - P$, which has dropped further to -36 Gt during the first day, starts to increase, as evaporation rates become larger than precipitation rates. Ten days backward in time, accumulated $E - P$ was greater than -11 Gt, indicating that more than two-thirds of the minimum $E - P$ of -36 Gt was accounted for by net evaporation. In other words, the net moisture uptake during these 10 days was about two-thirds of the estimated precipitation amount during the day before and upon arrival at the target. Evaporation E grows to a total accumulated value of about 55 Gt 10 days before the event, more than the minimum $E - P$ of -36 Gt. This indicates that more water than required for producing the precipitation had evaporated during the previous 10 days, and some of it was precipitated out before reaching the target. Indeed, there was precipitation diagnosed also en route, giving a total precipitation for the entire 10 days close to 70 Gt. However, the values for E and P must be interpreted with caution, because both are biased high.

5. Conclusions

In this paper we have described and validated a new Lagrangian method to diagnose the surface freshwater flux using atmospheric analysis data from ECMWF. With this method, the atmosphere is homogeneously ''filled'' with so-called particles, each of which carries an equal fraction of the total atmospheric mass. The particles move around along Lagrangian trajectories that are calculated using the winds from the meteorological analysis fields and parameterizations for turbulence. Specific humidity is interpolated from the analysis grid to the trajectory positions, and its changes along a trajectory are used to diagnose the net change of the water content of that particle due to the combined effects of evaporation and precipitation. Summation over all particles residing in an atmospheric column then yields the net surface freshwater flux $E - P$. Under the assumption that evaporation E and precipitation P do not coexist, E and P can also be diagnosed independently from each other. The method was compared with its Eulerian analog and also with precipitation and evaporation forecasts and observed precipitation. These comparisons were done for a 1-yr period and for a case study of an extreme precipitation event that caused severe flooding in central Europe.

In contrast to the equivalent existing Eulerian budget method (e.g., Trenberth 1997), the Lagrangian method can also be used only for select particles (e.g., those producing strong precipitation) and, thus, moisture and its sources and sinks can be tracked along these particles' trajectories. This can be used, for instance, to determine where the water that later became precipitation in a particular target region has evaporated. Moisture tracking was demonstrated at the example of the case study, in order to find out where the water producing the strong precipitation came from. Our main conclusions are as follows:

- When the Lagrangian method is used for the full set of particles, representing the total atmospheric mass, results are almost identical to those of the Eulerian budget method. A correlation between the results of the two methods explains 94% of the variance of the data and reveals no bias. This confirms the validity of the approach and the accuracy of its numerical implementation.
- Both methods yield patterns of the surface freshwater flux $E - P$ that are highly correlated to those obtained from evaporation and precipitation forecasts. However, the forecast moisture budget is unbalanced and has a global annual average precipitation surplus of 145 mm, whereas the diagnosed $E - P$ budgets are globally balanced.
- Diagnosing E and P independently from each other is possible only with a rather high level of noise. This leads to systematic overestimates of both, particularly in regions where both E and P are small. However, precipitation can be reliably diagnosed in regions where it is strong and for individual strong precipitation events. This is important because it allows the reliable identification of precipitation-producing particles.
- With the Lagrangian method, comprehensive source–sink relationships can be established that are not restricted to the calculation of local precipitation recycling ratios. Detailed maps of source contributions can be constructed.
- In a study of the extreme precipitation event that oc-

curred over Europe in August 2002, precipitation-producing particles were tracked back in time, and the evaporation source regions of the water that became precipitation were identified. The major source region was the Mediterranean, but it was found that evaporation from land surfaces also contributed substantial amounts of water. This was partly due to the wet spell preceding the extreme rain event, which left large areas of Europe with already water-saturated soils and some regions inundated. It is likely that the ECMWF forecasts underestimated the severity of the flooding event because of insufficient evaporation from land surfaces under these unusually moist conditions.

- Having demonstrated the capabilities of our Lagrangian method, our next goal is to apply it systematically for different regions of the globe and over longer time periods in order to establish global source–sink relationships of water vapor.
- The largest remaining problem is the positive bias for both *E* and *P*. Overcoming this problem might require incorporating liquid water and ice content, assuming that evaporation can only occur close to the surface, smoothing *q* along the trajectories to filter out the most unrealistic fluctuations, or using forecast or observation data to constrain at least one of the two quantities.

Acknowledgments. ECMWF and the German Weather Service are acknowledged for permitting access to the ECMWF archives. We thank B. Rudolf from the Global Precipitation Climatology Centre at the German Weather Service for gridded daily rain rauge data for August 2002. Thanks are also due to three reviewers for their constructive comments that greatly helped in clarifying the presentation of the new method.

REFERENCES

Adler, R. F., and Coauthors, 2003: The Version-2 Global Precipitation Climatology Project (GPCP) Monthly Precipitation Analysis (1979–present). *J. Hydrometeor.,* **4,** 1147–1167.

Bosilovich, M. G., and S. D. Schubert, 2002: Water vapor tracers as diagnostics of the regional hydrological cycle. *J. Hydrometeor.*, **3,** 149–165.

——, Y. C. Sud, S. D. Schubert, and G. K. Walker, 2003: Numerical simulation of the large-scale North American monsoon water sources. *J. Geophys. Res.,* **108,** 8614, doi:10.1029/2002JD003095.

Brubaker, K. L., P. A. Dirmeyer, A. Sudradjat, B. S. Levy, and F. Bernal, 2001: A 36-yr climatological description of the evaporative sources of warm-season precipitation in the Mississippi River basin. *J. Hydrometeor.,* **2,** 537–557.

Chen, T.-C., and J. Pfaendtner, 1993: On the atmospheric branch of the hydrological cycle. *J. Climate*, **6,** 161–167.

Crimp, S. J., and S. J. Mason, 1999: The extreme precipitation event of 11 to 16 February 1996 over South Africa. *Meteor. Atmos. Phys.,* **70,** 29–42.

D'Abreton, P. C., and P. D. Tyson, 1996: Three-dimensional kinematic trajectory modelling of water vapour transport over Southern Africa. *Water SA,* **22,** 297–306.

Dirmeyer, P. A., and K. L. Brubaker, 1999: Contrasting evaporative moisture sources during the drought of 1988 and the flood of 1993. *J. Geophys. Res.,* **104,** 19 383–19 397.

Eckhardt, S., and Coauthors, 2003: The North Atlantic Oscillation controls air pollution transport to the Arctic. *Atmos. Chem. Phys.,* **3,** 1769–1778.

——, A. Stohl, H. Wernli, P. James, C. Forster, and N. Spichtinger, 2004: A 15-year climatology of warm conveyor belts. *J. Climate,* **17,** 218–237.

Eltahir, E. A. B., and R. L. Bras, 1996: Precipitation recycling. *Rev. Geophys.,* **34,** 367–378.

Emanuel, K. A., and M. Živković-Rothman, 1999: Development and evaluation of a convection scheme for use in climate models. *J. Atmos. Sci.,* **56,** 1766–1782.

Forster, C., and Coauthors, 2001: Transport of boreal forest fire emissions from Canada to Europe. *J. Geophys. Res.,* **106,** 22 887–22 906.

——, and Coauthors, 2004: Lagrangian transport model forecasts and a transport climatology for the Intercontinental Transport and Chemical Transformation 2002 (ITCT 2k2) measurement campaign. *J. Geophys. Res.,* **109,** D07S92, doi:10.1029/2003JD003589.

Grazzini, F., and G. van der Grijn, 2003: Central European floods during summer 2002. *ECMWF Newsletter,* No. 96, ECMWF, Reading, United Kingdom, 18–28.

Hanna, S. R., 1982: Applications in air pollution modeling. *Atmospheric Turbulence and Air Pollution Modelling: A Course Held in The Hague, 21–25 September 1981,* F. T. M. Nieuwstadt and H. van Dop, Eds., D. Reidel, 275–310.

Houghton, J. T., Y. Ding, D. J. Griggs, M. Noguer, P. J. van der Linden, X. Dai, K. Maskell, and C. A. Johnson, Eds., 2001: *Climate Change 2001: The Scientific Basis.* Cambridge University Press, 944 pp.

Huffman G. J., and Coauthors, 1997: The Global Precipitation Climatology Project (GPCP) Combined Precipitation Dataset. *Bull. Amer. Meteor. Soc.*, **78,** 5–20.

——, R. F. Adler, M. M. Morrissey, D. T. Bolvin, S. Curtis, R. Joyce, B. McGavock, and J. Susskind, 2001: Global precipitation at one-degree daily resolution from multisatellite observations. *J. Hydrometeor.,* **2,** 36–50.

James, P., A. Stohl, C. Forster, S. Eckhardt, P. Seibert, and A. Frank, 2003: A 15-year climatology of stratosphere–troposphere exchange with a Lagrangian particle dispersion model: 1. Methodology and validation. *J. Geophys. Res.,* **108,** 8519, doi:10.1029/2002JD002637.

Koster, R., J. Jouzel, R. Suozzo, G. Russell, W. Broecker, D. Rind, and P. Eagleson, 1986: Global sources of local precipitation as determined by the NASA/GISS GCM. *Geophys. Res. Lett.,* **13,** 121–124.

Lee, D., and J. Veizer, 2003: Water and carbon cycles in the Mississippi River basin: Potential implications for the Northern Hemisphere residual terrestrial sink. *Global Biogeochem. Cycles,* **17,** 1037, doi:10.1029/2002GB001984.

Lin, J. C., C. Gerbig, S. C. Wofsy, A. E. Andrews, B. C. Daube, K. J. Davis, and C. A. Grainger, 2003: A near-field tool for simulating the upstream influence of atmospheric observations: The stochastic time-inverted Lagrangian transport (STILT) model. *J. Geophys. Res.,* **108,** 4493, doi:10.1029/2002JD003161.

Liu, J., and R. E. Stewart, 2003: Water vapor fluxes over the Saskatchewan River basin. *J. Hydrometeor.,* **4,** 944–959.

Newell, R. E., N. E. Newell, Y. Zhu, and C. Scott, 1992: Tropospheric rivers?—A pilot study. *Geophys. Res. Lett.,* **19,** 2401–2404.

Peixoto, J. P., and A. H. Oort, 1992: *Physics of Climate.* American Institute of Physics, 520 pp.

Reale, O., L. Feudale, and B. Torato, 2001: Evaporative moisture sources during a sequence of floods in the Mediterranean region. *Geophys. Res. Lett.,* **28,** 2085–2088.

Rodean, H. C., 1996: *Stochastic Lagrangian Models of Turbulent Diffusion. Meteor. Monogr.,* No. 48, Amer. Meteor. Soc., 84 pp.

Rudolf, B., and J. Rapp, 2003: The century flood of the river Elbe in August 2002: Synoptic weather development and climatolog-

ical aspects. Quarterly Rep. of the Operational NWP-Models of the Deutscher Wetterdienst, Special Topic July 2003, Deutscher Wetterdienst, Offenbach, Germany, 7 pp.

——, T. Fuchs, U. Schneider, and A. Meyer-Christoffer, 2003: Introduction of the Global Precipitation Climatology Centre (GPCC). Deutscher Wetterdienst Rep., Offenbach am Main, Germany, 16 pp.

Schneider, E. K., B. P. Kirtman, and R. S. Lindzen, 1999: Tropospheric water vapor and climate sensitivity. *J. Atmos. Sci.,* **56,** 1649–1658.

Smirnov, V. V., and G. W. K. Moore, 2001: Short-term and seasonal variability of the atmospheric water vapor transport through the Mackenzie River basin. *J. Hydrometeor.,* **2,** 441–452.

Spichtinger, N., M. Wenig, P. James, T. Wagner, U. Platt, and A. Stohl, 2001: Satellite detection of a continental-scale plume of nitrogen oxides from boreal forest fires. *Geophys. Res. Lett.,* **28,** 4579–4582.

Stohl, A., and P. Seibert, 1998: Accuracy of trajectories as determined from the conservation of meteorological tracers. *Quart. J. Roy. Meteor. Soc.,* **124,** 1465–1484.

——, and D. J. Thomson, 1999: A density correction for Lagrangian particle dispersion models. *Bound.-Layer Meteor.,* **90,** 155–167.

——, and T. Trickl, 1999: A textbook example of long-range transport: Simultaneous observation of ozone maxima of stratospheric and North American origin in the free troposphere over Europe. *J. Geophys. Res.,* **104,** 30 445–30 462.

——, G. Wotawa, P. Seibert, and H. Kromp-Kolb, 1995: Interpolation errors in wind fields as a function of spatial and temporal resolution and their impact on different types of kinematic trajectories. *J. Appl. Meteor.,* **34,** 2149–2165.

——, M. Hittenberger, and G. Wotawa, 1998: Validation of the Lagrangian particle dispersion model FLEXPART against large scale tracer experiment data. *Atmos. Environ.,* **32,** 4245–4264.

——, S. Eckhardt, C. Forster, P. James, and N. Spichtinger, 2002: On the pathways and timescales of intercontinental air pollution transport. *J. Geophys. Res.,* **107,** 4684, doi:10.1029/2001JD001396.

——, and Coauthors, 2003: A backward modeling study of intercontinental pollution transport using aircraft measurements. *J. Geophys. Res.,* **108,** 4370, doi:10.1029/2002JD002862.

Thomson, D. J., 1987: Criteria for the selection of stochastic models of particle trajectories in turbulent flows. *J. Fluid Mech.,* **180,** 529–556.

Trenberth, K. E., 1997: Using atmospheric budgets as a constraint on surface fluxes. *J. Climate,* **10,** 2796–2809.

——, 1999: Atmospheric moisture recycling: Role of advection and local evaporation. *J. Climate,* **12,** 1368–1381.

——, and C. J. Guillemot, 1998: Evaluation of the atmospheric moisture and hydrological cycle in the NCEP/NCAR reanalyses. *Climate Dyn.,* **14,** 213–231.

——, A. Dai, R. M. Rasmussen, and D. B. Parsons, 2003: The changing character of precipitation. *Bull. Amer. Meteor. Soc.,* **84,** 1205–1217.

Ulbrich, U., T. Brücher, A. H. Fink, G. C. Leckebusch, A. Krüger, and J. G. Pinto, 2003a: The central European floods of August 2002. Part I: Rainfall periods and flood development. *Weather,* **58,** 371–376.

——, ——, ——, ——, ——, and ——, 2003b: The central European floods of August 2002. Part II: Synoptic causes and considerations with respect to climatic change. *Weather,* **58,** 434–441.

van Bebber, W. J., 1891: Die Zugbahnen der barometrischen Minima. *Meteor. Z.,* **8,** 361–366.

Vogelezang, D. H. P., and A. A. M. Holtslag, 1996: Evaluation and model impacts of alternative boundary-layer height formulations. *Bound.-Layer Meteor.,* **81,** 245–269.

Webster, P. J., 1994: The role of hydrological processes in ocean–atmosphere interactions. *Rev. Geophys.,* **32,** 427–476.

Wernli, H., 1997: A Lagrangian-based analysis of extratropical cyclones. II: A detailed case-study. *Quart. J. Roy. Meteor. Soc.,* **123,** 1677–1706.

White, P. W., Ed., 2002: IFS Documentation. ECMWF Report, Reading, United Kingdom. [Available online at http://www.ecmwf.int.]

Yamanaka, T., J. Shimada, and K. Miyaoka, 2002: Footprint analysis using event-based isotope data for identifying source area of precipitated water. *J. Geophys. Res.,* **107,** 4624, doi:10.1029/2001JD001187.